

Strategy of Enhancing the Volumetric Energy Density for Lithium–Sulfur Batteries

Ya-Tao Liu, Sheng Liu, Guo-Ran Li, and Xue-Ping Gao*

Lithium–sulfur (Li–S) batteries hold the promise of the next generation energy storage system beyond state-of-the-art lithium-ion batteries. Despite the attractive gravimetric energy density (W_G), the volumetric energy density (W_V) still remains a great challenge for the practical application, based on the primary requirement of Small and Light for Li–S batteries. This review highlights the importance of cathode density, sulfur content, electroactivity in achieving high energy densities. In the first part, key factors are analyzed in a model on negative/positive ratio, cathode design, and electrolyte/sulfur ratio, orientated toward energy densities of $700 \text{ Wh L}^{-1}/500 \text{ Wh kg}^{-1}$. Subsequently, recent progresses on enhancing W_V for coin/pouch cells are reviewed primarily on cathode. Especially, the “Three High One Low” (THOL) (high sulfur fraction, high sulfur loading, high density host, and low electrolyte quantity) is proposed as a feasible strategy for achieving high W_V , taking high W_G into consideration simultaneously. Meanwhile, host materials with desired catalytic activity should be paid more attention for fabricating high performance cathode. In the last part, key engineering technologies on manipulating the cathode porosity/density are discussed, including calendaring and dry electrode coating. Finally, a future outlook is provided for enhancing both W_V and W_G of the Li–S batteries.

is considered as one of the most promising candidates for the next generation of high energy storage system.

Since proposed in the 1960s,^[3] Li–S battery experienced an infancy stage in 1970–1990s, when researchers devoted to the fundamental redox reactions of sulfur in various electrolytes,^[4] and a flourishing period after 2000 when high performance was achieved through sulfur/carbon (S/C) cathode and sulfurized-polyacrylonitrile (SPAN) cathode in ether- and carbonate-based electrolytes, respectively.^[5] After 2009, great efforts have been made to further enhance Li–S battery, including fabricating conductive cathode,^[6] incorporating electrocatalyst,^[7] modifying separator,^[8] optimizing electrolyte,^[9] and protecting lithium anodes.^[10] The rational design of electrode structure with various carbon materials (1D, 2D, and 3D) greatly boosts the electrochemical performance of sulfur cathode.^[11] Although the cycle stability is still struggling with 100 cycles, the gravimetric energy density (W_G) of Li–S pouch


1. Introduction

High energy density is the primary concern for the most applications of energy storage, particularly for power sources in modern mobile society. In the past three decades, as a representative of high energy batteries, commercial lithium-ion (Li-ion) batteries have made great achievements with the energy density upgraded triply from 100 Wh kg^{-1} to around 280 Wh kg^{-1} . However, restricted by the intercalation chemistry of electrode materials, Li-ion batteries have almost approached the upper limit of their energy density ($\approx 350 \text{ Wh kg}^{-1}$).^[1] Lithium–sulfur (Li–S) battery, with sulfur as cathode and lithium as anode, offers high theoretical energy densities up to 2600 Wh kg^{-1} or 2800 Wh L^{-1} , based on mass or volume, respectively.^[2] Therefore, Li–S battery

cells has improved remarkably to promote the applications in which weight matters more than longevity. For example, Sion Power, a pioneer corporation in Li–S battery technology, has developed several prototypical Li–S cells with energy density of $350 \text{ Wh kg}^{-1}/325 \text{ Wh L}^{-1}$ for powering Airbus’s Zephyr 7 drone for an 11-day nonstop flight in 2014.^[12] Oxis Energy, another manufacture of Li–S battery, announced a new target of 500 Wh kg^{-1} in the near future after achieving $400 \text{ Wh kg}^{-1}/300 \text{ Wh L}^{-1}$ for e-Buses, trucks, and marine applications.^[13] Research institutions from China have also reported pouch Li–S cells with the energy density up to $400\text{--}600 \text{ Wh kg}^{-1}$ for the potential application in unmanned aerial vehicle.^[14] It is remarkable that the W_G of Li–S battery has exceeded that of the best Li-ion batteries ($250\text{--}300 \text{ Wh kg}^{-1}$) with Ni-rich oxide cathode from Contemporary Amperex Technology Co., Ltd. (CATL), a giant manufacture of Li-ion batteries (Figure 1). With such great advantages, Li–S battery is possible to compete with commercial Li-ion batteries in specific field where high W_G is the primary concern.

Despite the attractive high W_G , Li–S battery pales in comparison with Li-ion batteries in terms of volumetric energy density (W_V).^[18] Figure 1 compares W_V and W_G between Li–S and Li-ion batteries. With Ni-rich metal oxide as cathode, Li-ion batteries have already reached 700 Wh L^{-1} and can even exceed 1000 Wh L^{-1} for W_V when coupling with high capacity

Dr. Y.-T. Liu, Dr. S. Liu, Prof. G.-R. Li, Prof. X.-P. Gao
Institute of New Energy Material Chemistry
School of Materials Science and Engineering
Renewable Energy Conversion and Storage Center
Nankai University
Tianjin 300350, China
E-mail: xpgao@nankai.edu.cn

 The ORCID identification number(s) for the author(s) of this article can be found under <https://doi.org/10.1002/adma.202003955>.

DOI: 10.1002/adma.202003955

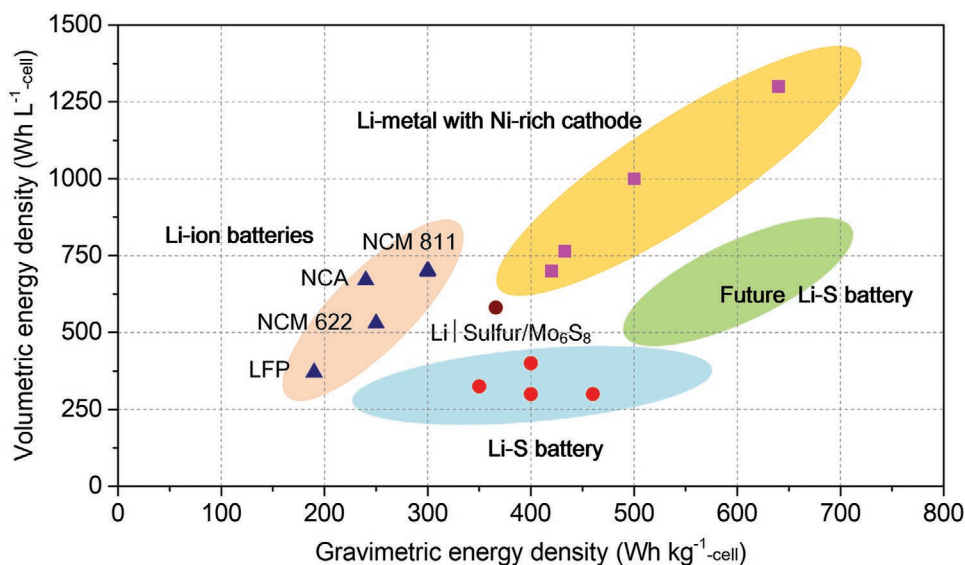


Figure 1. Comparison of W_V and W_G of Li-S battery, Li-ion batteries and lithium secondary batteries. The data (triangles) of $\text{LiNi}_{0.8}\text{Co}_{0.1}\text{Mn}_{0.1}\text{O}_2$ (NCM 811), $\text{LiNi}_{0.8}\text{Co}_{0.15}\text{Al}_{0.05}\text{O}_2$ (NCA), $\text{LiNi}_{0.6}\text{Co}_{0.2}\text{Mn}_{0.2}\text{O}_2$ (NCM 622), and LiFePO_4 (LFP) are from commercial Li-ion batteries of CATL, Panasonic, LG, and BYD companies, respectively. For Li-S battery, the data (circles) are collected from Sion Power,^[12a,15] Oxis Energy,^[13] and Liu group.^[16] The data (squares) of new lithium secondary batteries are obtained from Sion Power, with nickel-rich metal oxide as cathode material.^[15,17]

anodes.^[18b,19] In contrast, Li-S pouch cells are limited within 200–400 Wh L⁻¹ for W_V .^[16,20] It seems to be hard to achieve both high W_G and W_V for Li-S battery simultaneously under the current technologies. Such imbalance between W_V and W_G , altogether with the battery cycle life, makes people to exclude the possibility of Li-S battery as potential alternative to Li-ion batteries. In particular, Li-S battery would lose market interest in certain applications where high W_V is fundamental necessary, such as portable devices or electric vehicles.^[21] In these applications, batteries are required to provide enough energy in limited space. For example, apart from W_G , W_V is very sensitive to a smart phone in the palm. For electric vehicle, though high W_G is desired for driving heavy vehicles, the battery packs cannot occupy the manned space. Specifically, the total space designed for battery packs is ≈ 220 L for a car and 400 L for a sports utility vehicle.^[22] The newly emerging cell-to-pack technology from CATL, which skips the module process and directly integrate cells into packs, is just aimed at improving the space utilization for achieving higher energy densities.^[23] Even though W_G is satisfied for Li-S battery, it is still unrealistic to put a “fat” Li-S battery into the confined space to power a car. Therefore, both W_V and W_G are significant for the practical applications, based on the primary requirement of Small and Light for future Li-S battery. Researchers expect future Li-S battery to have W_V of 700 Wh L⁻¹ that is comparable to state-of-the-art Li-ion batteries (Figure 1).^[18a] Such advancement on W_V for Li-S battery can not only promote its application in niche market, such as drones or military fields, but also potentially make a great impact on the electric vehicle market.^[24] However, the W_V of 800 Wh L⁻¹ on the up edge in Ragone plot still looks like an impossible mission for Li-S battery based on the current technologies. As a result, W_V is a great challenge for further development of Li-S battery at current stage.^[18a]

However, the challenge on W_V has not attracted enough attention yet, although a few papers have pointed out this issue.^[18a,20,25] Since 2010, more than 6000 papers on Li-S battery have been published, and the vast majority of them has focused on W_G and cycling. Whereas in fact less than 60 papers are concerned about the W_V issue. This not only means the awkward situation of W_V at present, but also may mislead the research direction in future. To improve the W_V of Li-S battery, several important attempts have been made, which can be simply classified into two categories, i.e., high content of active sulfur and high density of sulfur cathode. For example, increasing the fraction of active sulfur and reducing the inactive materials in cathode are effective to enhance the overall discharge capacity.^[26] Freestanding type electrode without current collectors can further increase the energy output for the whole cathode.^[27] Introducing high density host materials,^[28] designing compact electrode structure,^[29] and employing calendaring technology^[30] are helpful to improve the cathode density. Specifically, as reported in many publications, metal oxides/sulfides/carbides, with higher densities than carbon materials,^[31] are demonstrated to be effective for improving the cathode density and accelerating the reaction kinetics simultaneously. Furthermore, some metal chalcogenides exhibit a similar electrochemical window (vs Li/Li⁺) to sulfur, and thus contribute extra capacity by acting as active materials.^[32]

As aforementioned, W_V is more important than W_G in some commercial applications of batteries, such as portable devices and electric automobiles.^[25] Therefore, W_V , as one of the basic requirements for energy storage system, should receive more or at least as much attention as W_G and cycle stability.^[21] Attaching enough importance to W_V , as well as W_G and cycle stability, will lead to a more promising Li-S battery. To this end, the present review highlights the significance of W_V and establishes a mathematical model to analyze key factors of dominating W_V

for Li–S battery. Besides, this review summarizes recent progress on W_V for both coin and pouch Li–S cells, and discusses the possible engineering technologies used for tuning the pore structure of sulfur cathode, with a special focus on the complex effect of calendaring on cathode density as well as sulfur redox. In particular, a “Three High One Low (THOL)” strategy is proposed in this review for achieving both high W_V and W_G . In the last part of the review, practical strategies are provided for the improvement of W_V in Li–S battery.

2. Key Factors of Dominating W_V of Li–S Battery

2.1. The Influence of N/P Ratio and Sulfur Cathode

Table 1 illustrates the differences in the cathode between Li–S and Li-ion batteries with respect to areal loading and mass fraction of active material, cathode density, porosity, as well as W_V based on cathode and cell volume. Comparing with the commercial $\text{LiNi}_x\text{Co}_y\text{Mn}_{1-x-y}\text{O}_2$ cathode, sulfur cathode in pouch cells usually has a low active material loading ($\approx 5 \text{ mg cm}^{-2}$) and fraction (50–70 wt%),^[33] which are restricted mainly by the poor ionic/electronic conductivities of the thick electrode. In particular, due to the high porosity ($\approx 70\%$) and low density ($\approx 0.5 \text{ g cm}^{-3}$) of sulfur cathode, W_V for Li–S battery is far behind that of Li-ion batteries no matter whether lithium or graphite are used as anode materials. This suggests that W_V of Li–S battery highly depends on the porosity and density, which are the key factors for dominating the cathode volume. Therefore, one effective strategy to enhance W_V is to fabricate a highly compact sulfur cathode, with high sulfur content for ensuring high W_G .

Essentially, the low density of sulfur cathode stems from the active sulfur itself. Thermally stable α -sulfur has a true density and tap density of 2.07 and $\approx 1.0 \text{ g cm}^{-3}$, respectively, which are much lower than those of the ternary oxide $\text{LiNi}_x\text{Co}_y\text{Mn}_{1-x-y}\text{O}_2$ cathode (≈ 4.7 and $\approx 2.5 \text{ g cm}^{-3}$, respectively), apart from the even lighter Li_2S with a true density of 1.66 g cm^{-3} . More severely, large amounts of carbon nanomaterials (nearly 30 wt%) are generally introduced into cathode as sulfur host for good utilization of active material. The light-weight carbon nanomaterials, with a low tap density of $\approx 0.1 \text{ g cm}^{-3}$, further results in low density and high porosity of cathode. Besides sulfur cathode, lithium excess and electrolyte quantity, characterized by negative/positive (N/P) ratio and electrolyte/sulfur (E/S) ratio, also influence the W_V of a full Li–S cell,^[18b,20,34] and will be discussed in the following text.

Due to complexity of Li–S battery, it is essential to include all the key parameters of dominating W_V in a mathematical model, such as density, porosity, sulfur loading, and fraction on

the sulfur cathode, N/P ratio, and E/S ratio. **Figure 2a** shows the schematic illustration of a prismatic Li–S pouch cell consisting of multilayer sulfur cathodes and lithium anodes with double side coating. To simplify the analysis, a single battery model, consisting of Cu foil, lithium anode, separator, sulfur cathode, and Al foil is adopted for calculation and discussion (**Figure 2b**). In this model, the electrode slurry is coated on single side of current collectors, and therefore the thickness of Al/Cu foils is calculated as a half of the real value. With this model, we propose that W_V can be derived by

$$W_V = \frac{U \cdot m_{\text{S-areal}} \cdot q_{\text{S}}}{d_{\text{cathode}} + d_{\text{Li}} + d_{\text{Al}} + d_{\text{Cu}} + d_{\text{separator}}} \quad (1)$$

in which U is the nominal voltage (2.1 V), $m_{\text{S-areal}}$ is the areal sulfur loading with single side coating (mg cm^{-2}), q_{S} is the average specific capacity of sulfur (1000 mAh g^{-1}), d_{cathode} , d_{Li} , d_{Al} , d_{Cu} , and $d_{\text{separator}}$ are thickness of cathode, lithium anode, aluminum foil (7.5 μm), copper foil (4.5 μm), and separator (15 μm), respectively. According to International Union of Pure and Applied Chemistry (IUPAC), the symbol W is adopted to represent the energy capacity (work) of a practical cell upon discharge under specified conditions.^[36] In literatures, symbol E is sometimes used for the cell energy, which should be noted to avoid confusion.^[18b,20,32b,37]

The calculated W_V would be a little higher than that of a real cell due to the absence of the integrated consideration. Equation (1) is founded based on three optimistic assumptions: 1) No cell swelling occurs; 2) Electrode volume remains unchanged upon cycling; 3) Electrolyte is accommodated in the pores of cathode and separator (ideally, lithium has no pore structures), and does not takes up extra volume. In practice, cell swelling possibly occurs because of the side reactions between ethereal solvents and lithium that generate volatile decomposition products, such as CH_4 and H_2 .^[35b,38] Conversion-type sulfur cathode and lithium anode suffer large shrinkage or expansion upon cycling. After coupling together, their volume change can offset each other and the pouch cell has maximum volume at full charge state and reaches minimum volume at the end of discharge. The volume variation is around 5% and can be controlled by limiting the voltage range.^[35a] The effect of electrolyte is a little bit complicated. Lean electrolyte, which is often the case for pouch Li–S cells, makes assumption 3) reasonable and Equation (1) valid. If flooded electrolyte is used, the effect of electrolyte will be non-negligible, which will be discussed separately in Section 2.2. Therefore, despite the rather optimistic assumptions, Equation (1) still offers rational analysis of key parameters that dominate W_V of a full Li–S cell.

Table 1. Comparison of Ni-rich intercalation cathode and sulfur cathode.

Characteristics	Active material loading [mg cm^{-2}]	Active material fraction [wt%]	Density [g cm^{-3}]	Porosity [%]	$W_{V\text{-cathode}}$ [Wh L^{-1}]	$W_{V\text{-cell}}$ [Wh L^{-1}]	
						With lithium	With graphite
$\text{LiNi}_x\text{Co}_y\text{Mn}_{1-x-y}\text{O}_2$ cathode	17	80–90	3	30	2000	1000	750
Sulfur cathode	5	50–70	0.5	70	880	550	410

Density and porosity are two critical parameters to dominate the cathode volume. Density refers to the ratio of mass to the apparent volume, and porosity (ϵ) is the ratio of pore volume to the apparent volume, which is calculated by^[39]

$$\epsilon = 1 - \frac{m_{\text{areal}} \cdot \sum \frac{w_i}{\rho_i}}{d_{\text{electrode}}} \quad (2)$$

in which m_{areal} is the areal loading of electrode (mg cm^{-2}), including sulfur, host, conductive agent, and binder, but not the current collector. w_i and ρ_i are mass fraction (wt%) and true density (g cm^{-3}) of the individual electrode component. $d_{\text{electrode}}$ is the electrode thickness (μm) without the current collector. The mass density (ρ) of cathode is related to the porosity by

$$\epsilon = 1 - \rho \cdot \sum \frac{w_i}{\rho_i} \quad (3)$$

For a conventional S/C cathode consisting of 70 wt% sulfur, 20 wt% carbon nanotube (CNT), and 10 wt% poly(vinylidene fluoride) (PVDF), one can easily obtain the slope (≈ 0.4846) using Equation (3), as listed in Table S4 (Supporting Information).

In order to use the above model, we first estimate the N/P ratio. Apparently, the ideal case would be the perfect capacity matching of lithium and sulfur (N/P ratio = 1). However, the metallic lithium acts as both the anode active material and current collector. It means that N/P ratio must be higher than 1, resulting in the reduction of the energy density (Figure 2d). Meanwhile, as lithium reservoir, metallic lithium anode suffers capacity loss due to its high sensitivity to organic electrolytes and inhomogeneous dissolution/deposition reactions, so that the excess lithium must be required to compensate the capacity loss. Therefore, N/P ratio is usually set to be near 2 in battery system, namely 100% lithium excess, which will be used in the following discussion of Section 2.1. and 2.2.

The dependence of W_V on sulfur is shown in Figure 2e. Higher sulfur loading or fraction means more active materials in the cell and will no doubt enhance the energy density. Assuming the specific capacity of sulfur is 1000 mAh g^{-1} , a frequently reported value in literatures, W_V increases remarkably with increasing sulfur loading below $\approx 6 \text{ mg cm}^{-2}$. For example, if the cathode density is 0.6 g cm^{-3} ($\approx 71\%$ porosity), a typical value for the state-of-the-art S/C cathode,^[30b,31b] W_V is estimated as 550 Wh L^{-1} at the sulfur loading of 6 mg cm^{-2} and the sulfur fraction of 70 wt%. When the sulfur loading exceeds 6 mg cm^{-2} , W_V gradually reaches a plateau regardless of sulfur

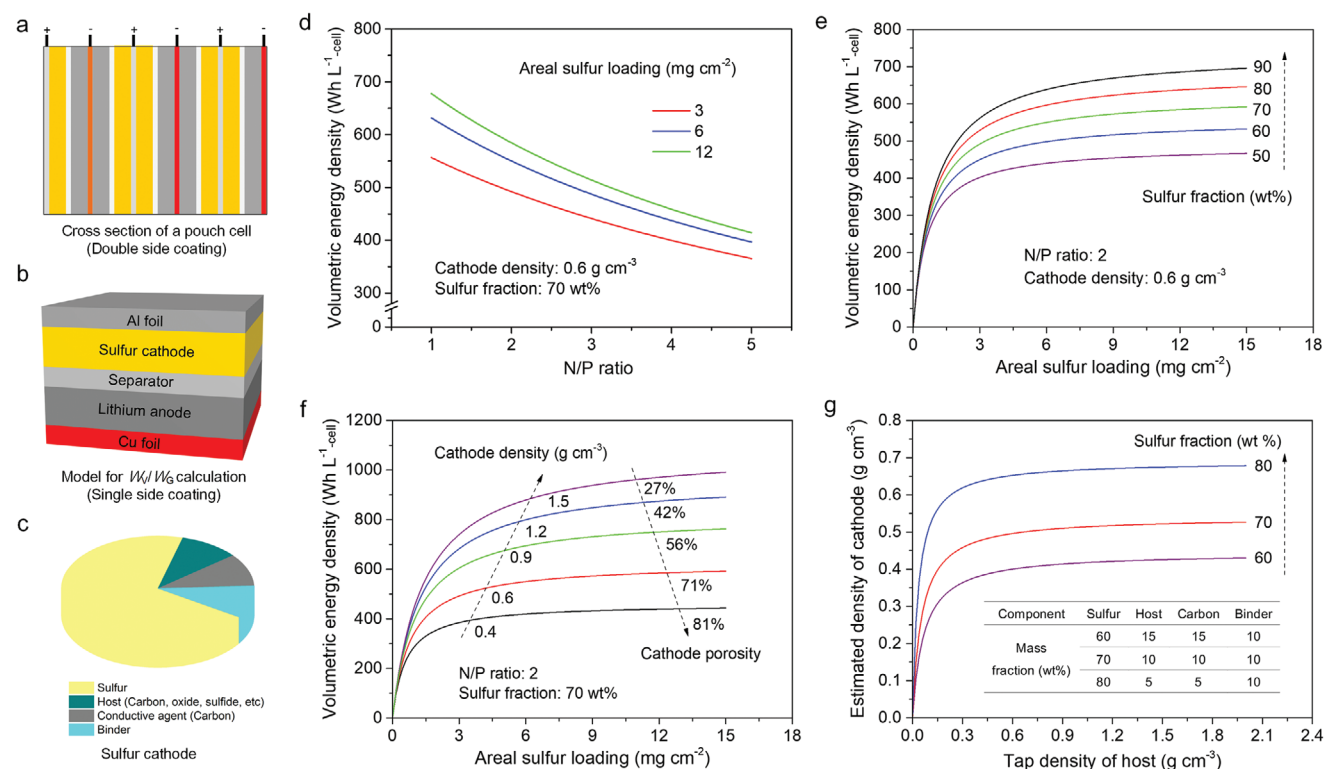


Figure 2. Key factors of dominating W_V of Li-S battery: Influences of N/P ratio and sulfur cathode. a) Schematic of cross section of a pouch Li-S cell showing the multilayer cathodes/anodes with double side coating. b) A simplified cell model for calculating energy density, in which cathode and anode are coated on the single side of Al or Cu current collectors. In this case, the thickness of current collectors is calculated as a half of the real thickness in pouch cell. c) Schematic of sulfur cathode consisting of sulfur, host, conductive agent and binder. d) Dependence of W_V on N/P ratio at different areal sulfur loadings. e) Dependence of W_V on areal sulfur loading and sulfur fraction. f) Dependence of W_V on areal sulfur loading and cathode density or porosity. g) Dependence of cathode density on the tap density of host materials and sulfur fraction of a cathode. To simplify the analysis, the calculation in this review uses only the cell volume before discharge without considering the volume change caused by cathode expansion and lithium shrinkage upon discharging. It should be noted that in practical electrode expansion/shrinkage and gaseous formation will alter the cell volume to some extent.^[33]

fraction. This implies that further increase of sulfur loading cannot enhance W_V anymore, and we will call this the “plateau effect.” Given the utilization of sulfur decreases with increasing sulfur loading and fraction, it seems impossible for Li–S cells to reach 600 Wh L⁻¹ by using the S/C cathode. Then, the cathode density or porosity begin to play a more influential role on W_V . Figure 2f shows the dependence of W_V on cathode density, in which sulfur fraction is set to be 70 wt%. In the sulfur loading of 6 mg cm⁻², for instance, if the cathode density is increased to 0.9 g cm⁻³ (≈56% porosity) or 1.2 g cm⁻³ (≈42% porosity), W_V can possibly reach 700 or 800 Wh L⁻¹, comparable to that of Li-ion batteries. Interestingly, the “plateau effect” become less prominent at higher cathode density, indicating that higher sulfur loading is feasible to further enhance W_V in this case. Specifically, W_V can even reach 900 Wh L⁻¹ when the cathode density is raised to 1.5 g cm⁻³ (≈27% porosity) at 7 mg cm⁻² sulfur loading. Note that ultrathin lithium foil below 30 μm is currently unavailable in industrial manufacture,^[34] the W_V below 3 mg cm⁻² sulfur loading would be very optimistic.

Given the high dependence of W_V on cathode density, the next question is how to effectively increase the cathode density. Generally, increasing the densities of all the components would be helpful for achieving this purpose (Figure 2c). Here, the tap density is introduced for the basic analysis. Tap density refers to the apparent density of powder material, which can be easily measured by the ratio of mass and volume after mechanically tapping the graduated cylinder or vessel with powder materials. Thus, the mass density of the cathode (ρ) can be roughly estimated according to the mass balance as^[31b]

$$\frac{1}{\rho} \approx \sum \frac{w_i}{\rho_{i\text{-tap}}} \quad (4)$$

where $\rho_{i\text{-tap}}$ is the tap density of each component within the cathode, including composite powder, binder, and conductive agent. Here, the cathode is the integral electrode (without current collector) that is prepared by conventional slurry casting without calendaring process. The estimated cathode density from Equation (4) is lower, but close to the real value.^[31b] The difference can be attributed to the following factors, i.e., the porous electrode architecture of different components and adhesive effect of binder. In this review, the sulfur-based composite and the corresponding tap density appear frequently. To avoid confusion, the sulfur-based composite refers in particular to the composite materials of sulfur and host materials (i.e., carbon, oxide, or sulfide) prepared by melt diffusion or chemical deposition, and the tap density of composite powder is measured as aforementioned.

Considering that sulfur, conductive carbon (CNT), and binder (PVDF), with tap densities of ≈1, 0.1, and 0.5 g cm⁻³, are usually permanent and hard to change, the feasible solution to tune the cathode density is to change the host materials.^[31a,b] The relationship between cathode density and tap density of host is shown in Figure 2g. Similar to the dependence of W_V on the sulfur loading, two regimes are observed with respect to the density relationship. Below ≈0.5 g cm⁻³, the cathode density increases sharply with increasing tap density of host. Above ≈0.5 g cm⁻³, “plateau effect” appears, meaning that the cathode density does not change much with further increasing

tap density of host. This inspires us that, on the one hand, increasing the tap density of host is effective in enhancing the cathode density; but on the other hand, chasing the highest tap density of host materials is not a wise strategy for host selection. When the density plateau appears, other criteria, including conductivity, adsorption ability and catalytic activity should be considered in order to make the cathode more electroactive. What's more, higher sulfur fraction also favors a higher cathode density because sulfur generally has a larger tap density than other components (i.e., conductive carbon and binder).

2.2. The Influence of E/S Ratio

Electrolyte quantity is an important parameter for full Li–S cell. As aforementioned, Equation (1) is valid under lean electrolyte conditions. If flooded electrolyte is incorporated, electrolyte will exert some effects on W_V because it takes up extra volume in the cell. To elucidate such effect, an assumption is first made, i.e., electrolyte fills into the pores of cathode and separator with priority and then the gaps between separator and electrodes. Lithium anode is considered as completely compact without any pore structures. The minimum electrolyte quantity filling up the pores is defined as the E/S threshold, which is porosity- or density-dependent and shows limited dependence on areal sulfur loading (Figure 3a). For a cathode with 6 mg cm⁻² sulfur loading and 70 wt% sulfur fraction, the E/S threshold for 71%, 56%, and 42% porosity is 1.8, 1.0, and 0.6 μL mg⁻¹, respectively. Note that the E/S threshold should change with the porosity variation of sulfur cathode upon cycling, and here only the full-charge state is considered to simplify the discussion.

When E/S ratio exceeds the threshold, the calculation of W_V can be given by amending equation (1) as

$$W_V = \frac{U \cdot m_{S\text{-areal}} \cdot q_S}{d_{\text{cathode}} + d_{\text{Li}} + d_{\text{Al}} + d_{\text{Cu}} + d_{\text{separator}} + d_{\text{electrolyte}}} \quad (5)$$

in which $d_{\text{electrolyte}}$ refers to the thickness of electrolyte. Clearly, W_V declines remarkably with electrolyte quantity (Figure 3b), thus suggesting the necessity of reducing E/S ratio. Also, it is interesting to note that W_V in this case is independent of cathode porosity or density, as shown by the completely overlapping curve for 6 mg cm⁻² sulfur cathode. This is a universal phenomenon and can be easily understood if electrolyte and cathode are taken as a whole. Equation (S17) (Supporting Information) confirms that when E/S ratio exceeds E/S threshold, the sum of cathode thickness and electrolyte thickness is a function of sulfur fraction and areal sulfur loading, with no relation with cathode porosity or density. To further elucidate the effect of electrolyte quantity, the relationship between E/S ratio and gravimetric energy density (W_G) is analyzed according to

$$W_G = \frac{U \cdot m_{S\text{-areal}} \cdot q_S}{\sum d_i \cdot \rho_i + (E/S \text{ ratio}) \cdot m_{S\text{-areal}} \cdot \rho_{\text{electrolyte}}} \quad (6)$$

in which d_i and ρ_i are the thickness and mass density of each part of the cell (cathode, anode, separator, Al foil, and Cu foil), respectively. $\rho_{\text{electrolyte}}$ is the mass density (≈1.1 g cm⁻³) of conventional ether electrolyte, i.e., 1 M LiTFSI and 2 wt% LiNO₃

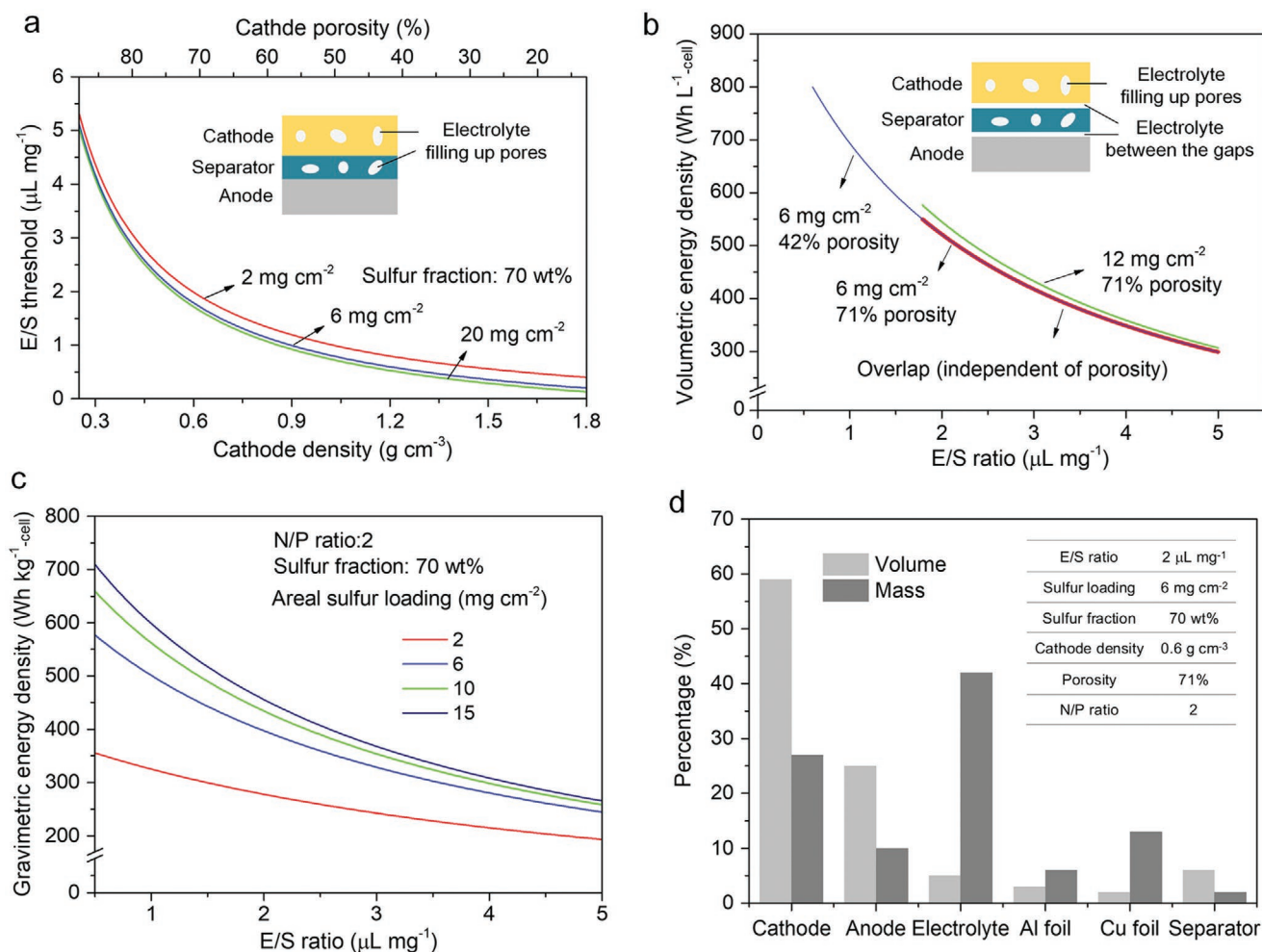


Figure 3. The influences of E/S ratio on W_V/W_C of Li-S battery. a) The minimum electrolyte quantity, or E/S ratio threshold, that fills up the pores of cathode and separator as a function of cathode density/porosity, based on the assumption that lithium surface is completely flat without pore structures. b) Dependence of W_V on electrolyte quantity when E/S ratio exceeds the threshold by assuming N/P ratio is 2 and sulfur fraction is 70 wt%. When excess electrolyte is used, electrolyte fills not only the pores of cathode and separator but also the gaps between electrode and separator, and thus takes up some volume of the cell. c) Dependence of W_C on E/S ratio and areal sulfur loading. d) Volume and mass fraction of each component (cathode, anode, electrolyte, Al foil, Cu foil, and separator) in a full Li-S cell at E/S ratio of 2 $\mu\text{L mg}^{-1}$. Sulfur cathode and electrolyte occupy the highest volume share (59%) and weight share (42%) of the full cell, respectively.

in 1,3-dioxolane (DOL)/1, 2-dimethoxyethane (DME) (1:1 by volume). The estimated energy density should be optimistic due to the absence of packages. It is shown in Figure 3c that low E/S ratio and high sulfur loading are both indispensable for high W_C . For a cell (6 mg cm^{-2} sulfur loading) to achieve 500, 400, and 300 Wh kg^{-1} , the minimum E/S ratio should be 1, 2, and 3.6 $\mu\text{L mg}^{-1}$, respectively. Figure 3d compares the mass and volume percentage of each component within a cell under 2 $\mu\text{L mg}^{-1}$ electrolyte, a value close to the common E/S ratio in pouch Li-S cells.^[30b,40] It is seen that cathode and electrolyte account for the biggest share of volume and mass, respectively, thus highlighting their critical role in dominating the W_V and W_C . In lean electrolyte of 2 $\mu\text{L mg}^{-1}$, the influence of electrolyte on W_V is limited, as shown by the low volume percentage ($\approx 5\%$) in Figure 3d. But this influence will become notable if excess electrolyte is used. At 2.5 and 3 $\mu\text{L mg}^{-1}$, the volume percentages of electrolyte sharply increase to 15.7% and 24.1%, respectively. This suggests that low E/S ratio is important to

both W_V and W_C of Li-S cells. Table 2 shows the critical parameters for achieving target energy densities, including sulfur loading, sulfur fraction, cathode density, cathode porosity as well as E/S ratio. Note that although low E/S ratio benefits the energy density, lean electrolyte Li-S cell still faces many problems because of the sluggish reaction kinetics and aggravated polysulfides shuttle, which is well addressed in some excellent papers^[41] and beyond the scope of this review.

3. Recent Progress on W_V of Li-S Battery

3.1. Li-S Coin Cells with Slurry Cast Cathode

Typically, sulfur, host, conductive agent, and binder are mixed to form an aqueous or nonaqueous slurry, which is then coated on the current collector to fabricate the slurry cast cathode. This technology is compatible with the large-scale production

Table 2. Representative energy densities at different parameters for Li–S battery.

Sulfur loading [mg cm ⁻²]	Sulfur fraction [wt%]	Cathode density [g cm ⁻³]	Cathode porosity [%]	E/S ratio [μL mg ⁻¹]	W _{V-cell} [Wh L ⁻¹]	W _{G-cell} [Wh kg ⁻¹]
4	60	0.6	71	3	390	290
6	70	0.6	71	3	420	330
6	70	0.9	56	3	420	330
6	70	0.9	56	2	520	400
6	70	1.2	42	2	520	400
6	70	1.2	42	1	700	500

of electrodes and is the most reported in literatures (Table 3). Unless otherwise noted, the current collector is not considered for calculating energy densities of cathode, as discussed in the text and in Table 3.

3.1.1. High W_V Based on Compact Carbon Host

Carbon nanomaterials, such as CNT, graphene, carbon fibers, and ketjen black (KB), are the most widely used hosts of sulfur due to the high conductivity, abundant pores, and high specific area. As aforementioned, although high W_G is obtained by using carbon nanomaterials as host materials, such light-weight hosts inevitably decrease the cathode density and W_V. Replacing the porous carbon with compact carbon could be a feasible approach to improve W_V.

For instance, Liu group designed a sandwich-type sulfur/graphene composite with functionalized graphene sheets/stacks.^[55] The composite, with 70 wt% sulfur, presents a high tap density of 0.92 g cm⁻³-composite, superior to the 0.35–0.40 g cm⁻³-composite of the conventional sulfur/mesoporous carbon composite, leading to the high volumetric capacity of 464 mAh cm⁻³-composite at 1C rate. Generally, microsized spheres possess the relatively high tap density due to the closely packed structure, and the contact resistance between microsized spheres could be reduced owing to the lower number of particle–particle interfaces.^[28] Inspired by this, Wang group prepared porous spherical carbon (PSC) with both microsized spherical morphology and hierarchical mesoporous structure using a combination of the emulsion polymerization and evaporation induced self-assembly method. The tap density of the S/PSC composite (75 wt%) is 1.08 g cm⁻³-composite, much higher than that of the S/super P composite (0.39 g cm⁻³-composite). Soon later, the high tap densities of 0.95 and 1.13 g cm⁻³-composite were also obtained by the same group for sulfur-based composites with CNT-interpenetrated N-doped carbon spheres (Figure 4a) and pyrolyzed polyacrylonitrile-KB, respectively.^[65] The high tap density can also be achieved by the space-efficient packing of nanosized primary particles in the microsized secondary particle, as demonstrated in the compact pomegranate-like carbon cluster-encapsulated sulfur cathode.^[51]

By tuning the pore structure, graphene can be used as sulfur host to achieve a high density.^[42,47,66] Yang group prepared a compact sulfur/reduced graphene oxide (S/rGO) composite utilizing H₂S as both sulfur source and reducing agent to trigger the self-assembly of rGO. The S/rGO composite has a high density up to 1.53 g cm⁻³-composite at a low sulfur fraction of 32 wt%.^[42] Graphene bulk materials with “ink-bottle-like” pores (Figure 4b)

have the advantage of high density (0.6–1.2 g cm⁻³) by compressing the pore percentage from 69% to 29%, superior to the light graphene or CNT (≈0.3 g cm⁻³).^[47] With the help of such compact graphene, the sulfur cathode with the sulfur loading of 5.3 mg cm⁻² and 54 wt% fraction shows the high density of 1.13 g cm⁻³-cathode, and high W_V of 1131 Wh L⁻¹-cathode based on the cathode volume. The similar dense integration of graphene can be also demonstrated in sulfur-based composites with the corresponding tap density as high as 1.265 g cm⁻³-composite.^[66]

Except for microsized or bulk carbon, the tightly packed nanosized carbon can also provide high density. For example, the compact sulfur cathode, with the interconnected close-packed N-doped porous carbon nanospheres as host (Figure 4c), presents the high density of 1.68 g cm⁻³-cathode and overwhelming W_V of 2619 Wh L⁻¹-cathode based on cathode volume.^[46] Owing to the highly ordered structures composed of metal ions and organic ligands, metal–organic-frameworks (MOFs) could derive heteroatom- and metal-doped carbon by carbonization or etching method without structural destruction. The refined structure makes these carbon materials suitable for compact host of sulfur. For instance, Kang group prepared 3D interconnected and open porous carbon by self-assembly of Zn, Co-bimetallic ZIF nanoparticles and following pyrolysis process (Figure 4d).^[29b] The resultant cathode exhibits the high density of 1.24 g cm⁻³-cathode at the sulfur loading of 10.3 mg cm⁻², and achieves the desirable W_V of 1777 Wh L⁻¹-cathode at 0.1C rate. When hollow N-doped carbon materials from imidazolium-based ionic polymer-encapsulated zeolitic imidazolate framework-8 are used as host, the high density of 1.36 g cm⁻³-cathode and high W_V of 1892 Wh L⁻¹-cathode can be obtained for the cathode under the sulfur fraction of 58.5 wt% and sulfur loading of 3.6 mg cm⁻².^[53]

For the light-weight carbon nanomaterials as host of sulfur, increasing sulfur fraction is also a feasible way to enhance the cathode density.^[67] As shown in Figure 4e, after increasing sulfur fraction from 54 to 90 wt%, the density of sulfur/aligned CNT composite can be increased gradually from 0.4 to 1.98 g cm⁻³-composite, leading to a marked improvement of W_V from 420 to 2232 Wh L⁻¹-cathode.^[26] In the case of the hybrid S/rGO-VS₂ composite, similar tendency is observed, where the tap density increases stepwise from 1.02 to 1.84 g cm⁻³-composite with increasing sulfur fraction from 64 to 89 wt%.^[57] To obtain a compact cathode, Nazar group reported a comprehensive approach by coupling a multifunctional and hierarchically structured sulfur composite with an in situ cross-linked binder (Figure 4f).^[29a] The in situ esterification results in a compact and crack-free sulfur cathode with a high sulfur loading up to 14.9 mg cm⁻² and decent electrochemical performance at low E/S ratio of 3.5 μL mg⁻¹. Correspondingly, the cathode

Table 3. Gravimetric/volumetric energy densities of slurry cast sulfur cathodes and corresponding full cells.

Sulfur host	C-rate	Sulfur loading [mg cm ⁻²]	Sulfur fraction [wt%]	Areal capacity [mAh cm ⁻²]	Cathode density [g cm ⁻³]	Cathode thickness [μm]	Voltage [V]	Cathode ^{a)}		E/S [μL mg ⁻¹]	Cell ^{b)}		Ref.
								W _V [Wh L ⁻¹]	W _G [Wh kg ⁻¹]		W _V [Wh L ⁻¹]	W _G [Wh kg ⁻¹]	
Graphene	0.5C	0.576	25.6	0.434	1.07	21	2.1	433.4	405	—	155	101	[42]
Super P/MWCNT	0.1C	1.5	80	1.1	0.83	22.6	2.1	≈1050	≈1260	—	396	232	[43]
Graphene/graphite	0.1C	3.6	55.3	—	—	—	2.1	1565	—	—	—	326	[44]
Ketjen black	0.01C	6	67.5	7.8	0.61	146	2.1	1132	1857	—	543	393	[45]
3D carbon network	0.1C	10.9	74	10.3	1.24	118	2.05	1777	1433	6	904	446	[29b]
Carbon nanospheres	0.05C	5	59.5	5.3	1.68	50	2.1	2249	1331	6	831	364	[46]
Ketjen black	0.1C	4	64	3.9	1.04	60	2.1	1360	1280	—	664	351	[30b]
Aligned CNT	0.1C	1.2	76.5	0.893	1.98	8	2.0	2232	1127	—	539	200	[26]
Dense graphene	0.1C	5.6	54	5.8	1.16	89	2.1	1371	1182	—	685	362	[47]
Carbon	0.1C	4	61	5.4	0.765	86	2.1	1319	1729	4	552	346	[48]
MWCNT	0.06C	4	64	4.73	0.52	120	2.1	828	1590	3.3	450	351	[16]
Ketjen Black	0.1C	3.5	64	3.5	0.68	80	2.1	919	1344	—	518	337	[49]
Acetylene Black	0.06C	6.7	75.4	7.5	0.74	120	2.1	1312	1773	5	660	414	[50]
Carbon cluster	0.2C	2	63	2.2	1.27	25	2.1	1848	1455	—	512	263	[51]
Super P	0.2C	1	49.3	1.02	0.95	21	2.1	1004	1054	—	268	166	[52]
Hollow carbon	0.1C	3.6	58.5	4.03	1.36	45	2.1	1892	1383	10	701	332	[53]
Carbon nanotiles	0.06C	—	65.3	—	1.5	—	2.1	1790	1193	—	—	—	[54]
Graphene	0.1C	—	56.8	—	1.6	—	2.1	1827	1133	—	—	—	[55]
Active Mo ₆ S ₈ (42.25 wt%)	0.05C	6.2	42.75	7.8	1.2	121	2.1	1217	1015	2.4	702	384	[32b]
La _{0.8} Sr _{0.2} MnO ₃	0.024C	6.2	65	7.2	1.7	54	2.05	2727	1551	7	901	392	[31b]
Organosulfur (70 wt%)	0.27C	7.07	70	5.05	2	51	1.96	1959	980	7.1	1001	410	[56]
Graphene/VS ₂	0.1C	2.56	71.2	2.6	1.64	22	2.1	2482	1515	10	681	305	[57]
Ti ₃ C ₂ T _x	0.03C	10.05	59	10.04	4.48	38	2.0	5281	1179	8	1286	412	[31c]
Ti ₃ C ₂ MXene	0.05C	13.8	64.2	13.7	3.7	58	1.95	4599	1243	10	1311	440	[58]
Graphite C ₃ N ₄	0.05C	5	60	4.27	0.56	150	2.1	602.5	1076	—	466	365	[59]
Graphene/C ₃ N ₄	0.06C	5.2	65.5	5.15	0.76	105	2.1	1035	1362	5	597	378	[29a]
Co(OH) ₂ /hydroxides	0.1C	3	52.5	3.04	1.27	45	2.1	1420	1118	—	620	304	[60]
CNT/TiS ₂	0.2C	2.8	68.9	2.24	0.9	45	2.1	1042	1158	10	576	315	[61]
LiNi _{0.8} Co _{0.1} Mn _{0.1} O ₂	0.1C	1	49	1.26	1.96	10.4	2.1	2550	1239	10	312	166	[62]
SPAN	0.1C	3.5	38.4	5.07	1.54	60	1.8	1528	992	10.4	609	289	[63]
SiO ₂	0.2C	4	52	3.8	1.77	44	2.1	1850	1046	15	764	331	[64]

^{a)}Without considering the current collector. The data are collected or derived from literatures; ^{b)}Renormalized energy densities based on full cell for better comparison. The full cell configuration adopts the model in Figure 2b. N/P ratio is set to be 2 for areal sulfur loading exceeding 3 mg cm⁻² and lithium foil of 30 μm is used for sulfur loading below 3 mg cm⁻². To simulate the practical pouch cell, a E/S ratio of 2 μL mg⁻¹ is assumed. Since the influence of lean electrolyte on W_V is limited (shown in Figure 3d), the calculation of W_V uses only cathode parameters, including the areal sulfur loading, sulfur fraction and cathode density according to Equation (1). Two cathode parameters (areal sulfur loading and sulfur fraction) and one electrolyte parameter (E/S ratio) are used for calculating W_G according to Equation (6).

has an improved density of 0.76 g cm⁻³_{-cathode} and W_V of 1035 Wh L⁻¹_{-cathode} at 0.06C rate.

3.1.2. High W_V Based on Carbon-Free or Hybrid Host

Carbon-free host materials refer to metal oxides, sulfides, nitrides and carbides herein. Compared with light-weight

carbon, carbon-free host intrinsically possesses a higher density and therefore has the natural advantage in fabricating a compact cathode, as discussed in Figure 2g. The tap densities of sulfur-based composites based on porous carbon, compact carbon, and carbon-free host are illustrated in Figure 5e. Introducing carbon-free host into cathode can date back to 2004, when Mg_{0.5}Ni_{0.5}O was utilized as a nanosized adsorbing additive,^[68] followed by a variety of materials, such as TiO₂,^[69]

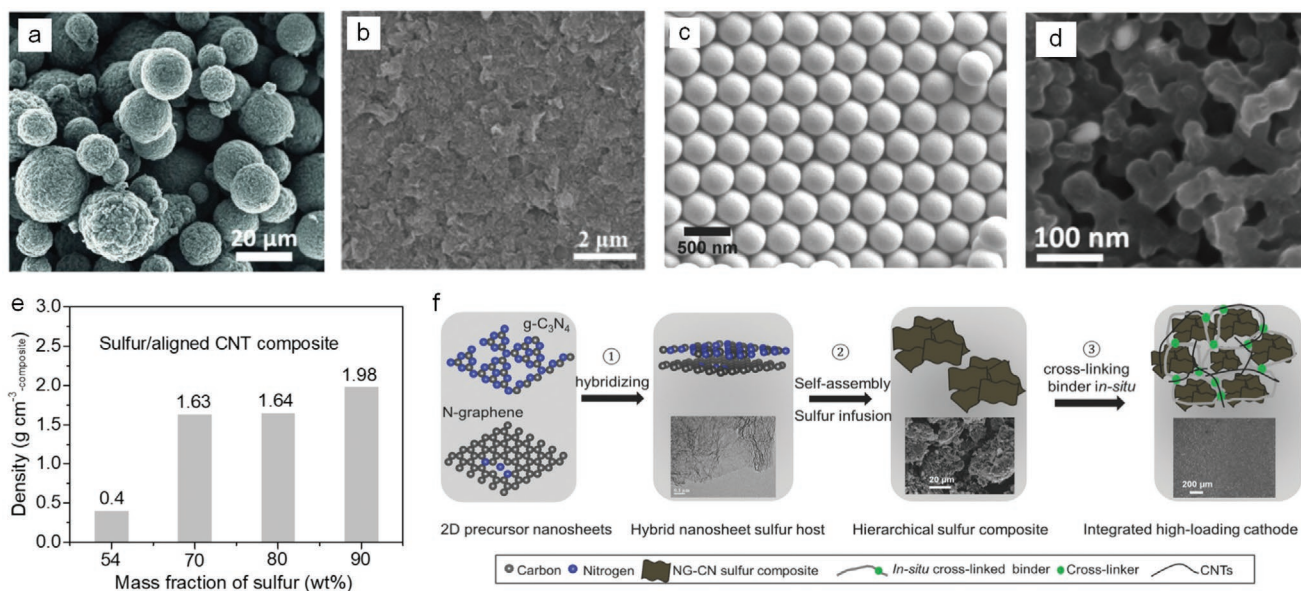


Figure 4. Compact carbon host to enhance W_V . a) Carbon-nanotube-interpenetrated mesoporous N-doped carbon spheres (MNCS/CNT). Reproduced with permission.^[65a] Copyright 2015, Wiley-VCH. b) High density graphene bulk materials with “ink-bottle-like” mesopores. Reproduced with permission.^[47] Copyright 2018, Wiley-VCH. c) Monodisperse nitrogen-doped carbon nanospheres (NCNS). Reproduced with permission.^[46] Copyright 2017, Wiley-VCH. d) SEM image of open porous 3D network derived from Zn, Co-bimetallic ZIF nanoparticles. Reproduced with permission.^[29b] Copyright 2018, Elsevier. e) Dependence of density of sulfur/aligned CNT composite on sulfur loading. Reproduced with permission.^[26] Copyright 2014, Elsevier. f) Schematic illustration of coupling hierarchical sulfur composite based on a hybrid host with in situ cross-linked binder for compact and thick sulfur cathodes. Reproduced with permission.^[29a] Copyright 2017, Wiley-VCH.

TiO₂,^[70] Ti₄O₇,^[71] MnO₂,^[72] CeO₂,^[73] MoS₂,^[74] VS₄,^[75] CoS₂,^[76] TiN,^[77] Co₃N,^[78] MgB₂,^[79] Pt,^[80] and Co.^[81] In most cases, these publications concentrate on the adsorption or catalysis role of carbon-free host materials without consideration of the densification effect. Usually, the metal compound nanomaterials are supported on carbon matrix to form a hybrid host for further improving the adsorption or catalysis effect.

More recently, heavy and catalytic metal compounds are introduced into carbon-free host materials to enhance the W_V for Li-S battery, including NiFe₂O₄,^[83] NiCo₂O₄,^[31a] CoOOH,^[82] LiNi_{0.8}Co_{0.1}Mn_{0.1}O₂,^[62] RuO₂,^[84] La_{0.8}Sr_{0.2}MnO₃,^[31b] and Nb₁₈W₁₆O₉₃ (Figure 5).^[85] These heavy metal oxides not only benefit the fabrication of the compact cathode, but also help to suppress the shuttle of soluble lithium polysulfides (LiPS) through the superior catalytic feature or adsorption ability. Taking La_{0.8}Sr_{0.2}MnO₃ nanofibers as example (Figure 5c), the metal oxide exhibits a high tap density up to ≈ 2.6 g cm⁻³. The good conductive framework constructed by nanofibers facilitates the high sulfur loading (65 wt% and >4 mg cm⁻²) and fast mass transfer of soluble LiPS. Correspondingly, the prepared compact S/La_{0.8}Sr_{0.2}MnO₃ cathode shows desired density and porosity of 0.98 g cm⁻³-cathode and 55%, respectively (Figure 5f).^[31b] Moreover, La_{0.8}Sr_{0.2}MnO₃ can serve as efficient electrocatalyst for facilitating the conversion of soluble LiPS by enhancing the diffusion, adsorption, and charge-transfer processes on the electrolyte/electrode interface. As a result, high W_V of 1787 Wh L⁻¹-cathode and high W_G of 1783 Wh kg⁻¹-cathode are obtained simultaneously for the S/La_{0.8}Sr_{0.2}MnO₃ cathode under the sulfur loading of 6.2 mg cm⁻² and electrolyte quantity of 7 μ L mg⁻¹ (Figure 5f). Besides, graphite C₃N₄,^[59] Co₉S₈,^[31d] Co(OH)₂/hydroxides,^[60] and CoMn₂O₄^[86] are also reported to

serve as carbon-free host materials. Also, MXene-based host materials were recently introduced into sulfur cathode by Wang group (Figure 5d).^[31c,58] The prepared flower-like Ti₃C₂T_x possesses a high electronic conductivity up to 10⁴ S cm⁻¹, so that it serves as both carbon-free host and conductive agent. The resultant S/Ti₃C₂T_x cathode synchronously acquires a high areal capacity of 10.04 mAh cm⁻² which corresponds to the ultrahigh W_V of 5281 Wh L⁻¹-cathode.

Combining carbon matrix and carbon-free nanoparticles to form a hybrid host is a common strategy in Li-S battery (Figure 6). The hybrid host inherits some of the unique advantages of their individual components, such as suitable conductivity, high density, and good catalytic/adsorption feature. For example, benefiting from the tightly stacked architecture and polar adsorption of VS₂, the elastic sandwich-structured S/rGO/VS₂ composite can accommodate the volume expansion upon cycling, and simultaneously exhibits a good electroactivity.^[57] Under high sulfur fraction of 89 wt%, the composite presents a high tap density of 1.84 g cm⁻³-composite, leading to high volumetric capacity of 1182.1 mAh cm⁻³-composite. Similarly, the mesoporous FePO₄/carbon as hybrid host is also helpful to fabricate the compact sulfur cathode with good cycling performance.^[87]

Although W_V can be enhanced through compact hosts, most of the hosts are electrochemically inert in the working window of Li-S battery, and thus sacrifice at least 10–20 wt% mass fraction of the cathode. Therefore, employing electrochemical active materials as sulfur host is also attempted recently. A variety of metal chalcogenides (oxides or sulfides) can react with lithium near the electrochemical window of S₈ (1.7–2.8 V, vs Li/Li⁺), as shown in Figure 7a. These materials are able to contribute extra

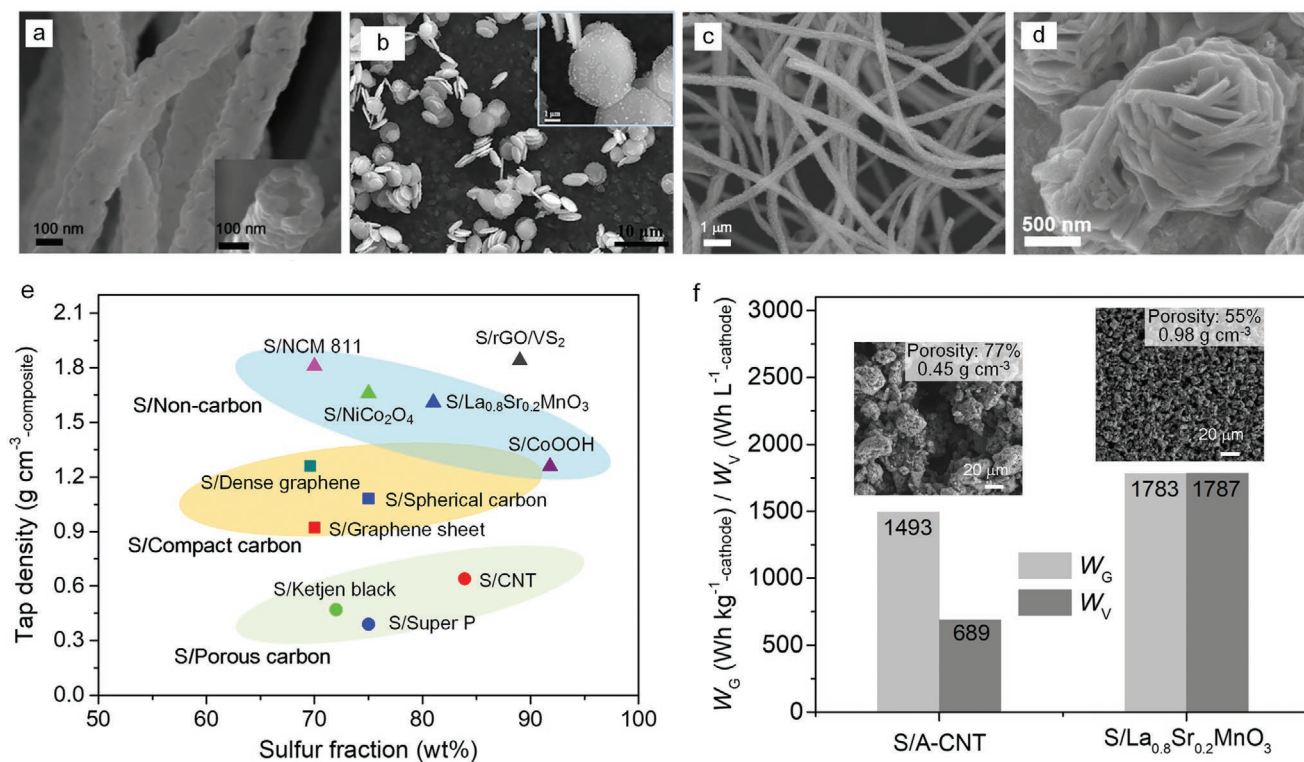


Figure 5. Heavy carbon-free host materials (metal oxides, sulfides, etc.) to improve W_V . SEM images of a) hollow NiCo_2O_4 nanofibers. Reproduced with permission.^[31a] Copyright 2019, Wiley-VCH. b) CoOOH sheets. Reproduced with permission.^[82] Copyright 2019, Wiley-VCH. c) $\text{La}_{0.8}\text{Sr}_{0.2}\text{MnO}_3$ nanofibers. Reproduced with permission.^[31b] Copyright 2020, Wiley-VCH. d) flower-like $\text{Ti}_3\text{C}_2\text{T}_x$. Reproduced with permission.^[31c] Copyright 2019, American Chemical Society. e) Tap density of different sulfur-based composites with porous carbon, compact carbon, and carbon-free host materials: S/Ketjen black,^[65b] S/Super P,^[28] S/CNT,^[83] S/Graphene sheet,^[55] S/Spherical carbon,^[28] S/Dense graphene,^[66] S/NCM 811,^[62] S/ NiCo_2O_4 ,^[31a] S/ $\text{La}_{0.8}\text{Sr}_{0.2}\text{MnO}_3$,^[31b] S/CoOOH,^[82] and S/rGO/VS₂.^[57] f) Comparison of W_V and W_G between S/ $\text{La}_{0.8}\text{Sr}_{0.2}\text{MnO}_3$ and sulfur/aligned carbon nanotubes (S/A-CNT) cathodes. The inset shows the SEM images of the compact S/ $\text{La}_{0.8}\text{Sr}_{0.2}\text{MnO}_3$ cathode and porous S/A-CNT cathode, and the density and porosity are also indicated. Reproduced with permission.^[31b] Copyright 2020, Wiley-VCH.

capacity by acting as active materials. Figure 7b shows the discharge–charge curves of S/ FeS_2/FeS composite in ether-based electrolyte, in which a sloped potential plateau is presented with a high specific capacity over 2000 mAh g^{-1} -sulfur based on sulfur mass.^[32a] The composite (sulfur: $\text{FeS}_2/\text{FeS} = 29.1:30$ by weight) exhibits a high tap density of 1.4 g cm^{-3} -composite, which corresponds to a compaction density of 2.04 g cm^{-3} -composite and an ultrahigh volumetric capacity of 2031 mAh cm^{-3} -composite after 30 cycles.^[32a] Li group and his co-workers adopted Mo_6S_8 , a cathode material for Mg and aqueous Li-ion batteries, as heavy and active host successfully (Figure 7c).^[32b] Mo_6S_8 undergoes an electrochemical reaction of $4\text{Li}^+ + 4e^- + \text{Mo}_6\text{S}_8 \leftrightarrow \text{Li}_4\text{Mo}_6\text{S}_8$ and delivers a theoretical specific capacity of 128 mAh g^{-1} in 1.7–2.8 V (vs Li/Li⁺).^[32b] Moreover, Mo_6S_8 possesses a good electronic/ionic conductivity, and exhibits high affinity for intermediate LiPS, making itself ideal backbone to immobilize sulfur as well as to ensure a good electrochemical performance. A typical S/ Mo_6S_8 hybrid cathode is composed of 42.75 wt% sulfur, 42.25 wt% Mo_6S_8 , 10 wt% carbon, and 5 wt% binder. With the compact structure and low porosity of 55%, the electrolyte/active materials (E/AM) ratio is decreased to $1.2 \mu\text{L mg}^{-1}$. Both high W_G and W_V (402 Wh kg^{-1} -cell and 731 Wh L^{-1} -cell) are achieved simultaneously with respect to the full cell volume and mass in the coin-cell configuration, outperforming state-of-the-art Li-ion batteries. In pouch cells (1 Ah) with multilayer

S/ Mo_6S_8 cathodes and lithium anodes ($\approx 2 \times$ excess lithium), high energy densities of 366 Wh kg^{-1} -cell and 581 Wh L^{-1} -cell are achieved. Besides, CuS ,^[90] VO_2 ,^[32c] RuO_2 ,^[84,91] and TiS_2 ^[92] have also been reported to serve as capacity-contributing hosts.

As noted in Figure 7a that heavy metal chalcogenides usually have limited specific capacity ($< 600 \text{ mAh g}^{-1}$) in comparison to light-weight sulfur ($\approx 1200 \text{ mAh g}^{-1}$). It means that the gravimetric capacity of cathode is dominated mainly by sulfur fraction, while the volumetric capacity of cathode is greatly related to the densification effect of heavy metal compounds. The capacity contribution from metal chalcogenides is not prominent until the mass fraction reaches a high level of $\approx 40 \text{ wt\%}$, which would sacrifice the sulfur fraction and hence the W_G . The advantages and disadvantages coexist in terms of introducing hybrid cathode into Li–S battery, and the optimization/design should be considered between W_V and W_G in battery.

3.1.3. High W_V Based on Sulfur-Rich Materials

As active material, sulfur takes up the highest mass fraction, and therefore the most significant impacts on the cathode density. Accordingly, a feasible strategy for enhancing cathode density is to replace sulfur with sulfur-rich materials that have a higher density than the elemental sulfur. Here,

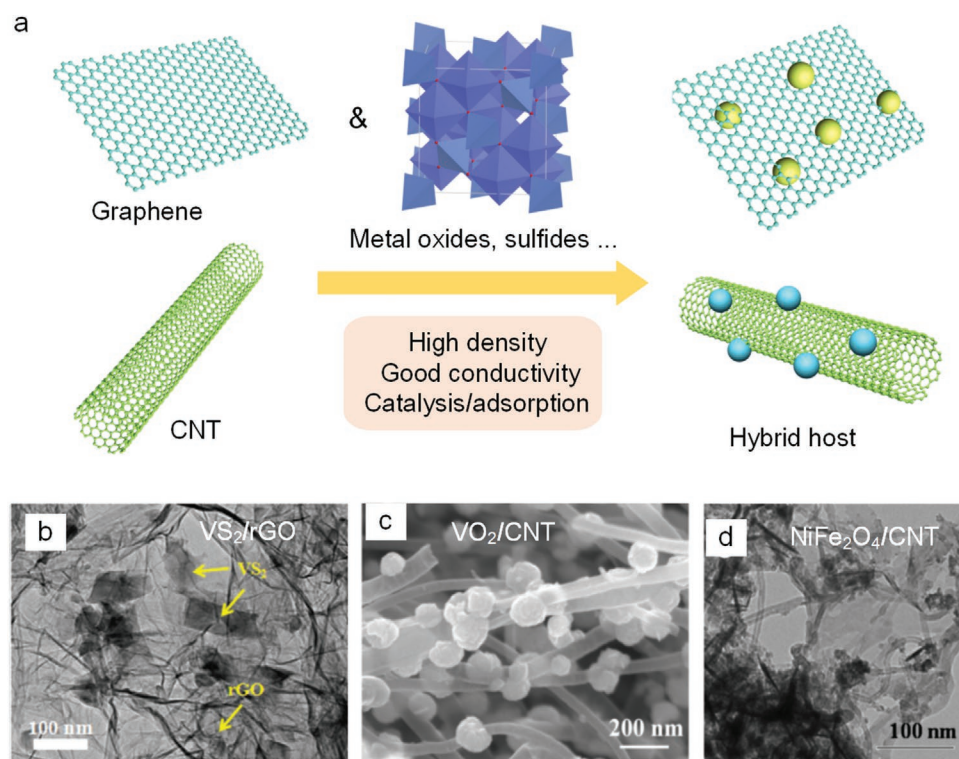


Figure 6. Hybrid host to improve W_V : a) Schematic illustration of metal oxide/sulfide nanoparticles on carbon matrix to form hybrid host that possesses both high density and good conductivity. b–d) Hybrid host. b) TEM image of VS_2/rGO . Reproduced with permission.^[57] Copyright 2018, Wiley-VCH. c) SEM image of VO_2/CNT . Reproduced with permission.^[88] Copyright 2019, Elsevier. d) TEM image of $NiFe_2O_4/CNT$. Reproduced with permission.^[89] Copyright 2015, American Chemical Society.

sulfur-rich materials refer to sulfur compounds or derivatives that have a high percentage of sulfur atom in the molecules and simultaneously possess a similar electrochemical behavior to that of sulfur. Such materials include sulfurized polymer,^[5a,101] organosulfur,^[102] sulfur–selenium solid solution (Se_xS_y),^[103] sulfur–tellurium (Te_xS_y),^[104] phosphor–sulfur compounds (P_2S_x),^[105] and metal polysulfides (MoS_3 , TiS_4 , and FeS_x).^[106] SPAN, first reported by Wang et al. in 2002, is a typical sulfurized-polymer with a sulfur fraction of ≈ 45 wt% and exhibits excellent lithium storage capability.^[5a,107] Sulfur in SPAN undergoes a solid–solid conversion and shows a slope discharge curve between 1.0 and 2.5 V (vs Li/Li^+).^[108] Amorphous MoS_3 , with a chainlike molecular structure of molybdenum ions bridged by sulfide and disulfide ligands (Figure 8a, inset), also serves as typical sulfur-rich material which displays similar voltage to that of the sulfur/microporous carbon or SPAN (Figure 8a).^[106a] Se_xS_y behaves more like elemental sulfur and shows the typical two voltage plateaus in ether electrolyte (Figure 8b).^[103a,b]

Sulfur-rich materials extend the category of cathode materials for Li–S battery. In particular, some sulfides as typical sulfur-rich materials, such as MoS_3 , SeS , TeS_3 , and TiS_3 , possess high theoretical densities of 3.72, 4.66, 4.297, and 2.94 g cm^{-3} , respectively (Table S19, Supporting Information).^[109] This provides a promising opportunity to fabricate dense cathodes owing to their inherent higher density than that of elemental sulfur (2.07 g cm^{-3}). Notably, as for the sulfur–selenium solid solution, Se can act as active materials in a similar working window (1–3 V, vs Li/Li^+) to sulfur.^[110] The theoretical gravimetric

and volumetric capacities of SeS are 968 mAh g^{-1} and 4510 mAh cm^{-3} , respectively. However, sulfurized polymer and organosulfur contain light chains/groups (including $-CH_3$, $-C-C-$, and $-C=N-$), which are not favorable for enhancing the density. By using a simple “back of the envelope” method proposed by Girolami,^[111] the true density of sulfur-limonene polysulfide (2 limonene units and 12 sulfur atoms in a molecule) is predicted to be $\approx 1.13 \text{ g cm}^{-3}$, only a half that of elemental sulfur. The true density of sulfurized polymer varies with sulfur content. The sulfurized polymer shows a high dispersion owing to the polydispersity of polymer molecules. Due to the lack of data in published literatures, the true density of SPAN here is roughly estimated using pure sulfur (2.07 g cm^{-3}) and pure PAN (1.187 g cm^{-3}) without considering the molecular configuration and bonding formation during pyrolysis. Thus, 48 wt% sulfur and 52 wt% PAN yield a true density of $\approx 1.52 \text{ g cm}^{-3}$ for SPAN. Obviously, light-weight sulfur-rich material is not a good choice in terms of enhancing the cathode density.

Good demonstration for enhancing W_V through heavy sulfur-rich materials is given in selenium-doped poly(diallyl terasulfide) (PDATtSSe) system.^[56] which can be directly reduced to short-chain lithium sulfide and selenium products (Li_2SSe , Li_2S_2Se , $RSLi$, RS_2Li , RS_2SeLi), without forming long-chain LiPS in ether-based electrolyte. PDATtSSe undergoes a similar reaction pathway to SPAN, but exhibits a higher and more flat voltage plateau during discharge (Figure 8c). Importantly, PDATtSSe has a really high tap density of 3.51 g cm^{-3} .^{PDATtSSe}, and the resultant cathode density reaches

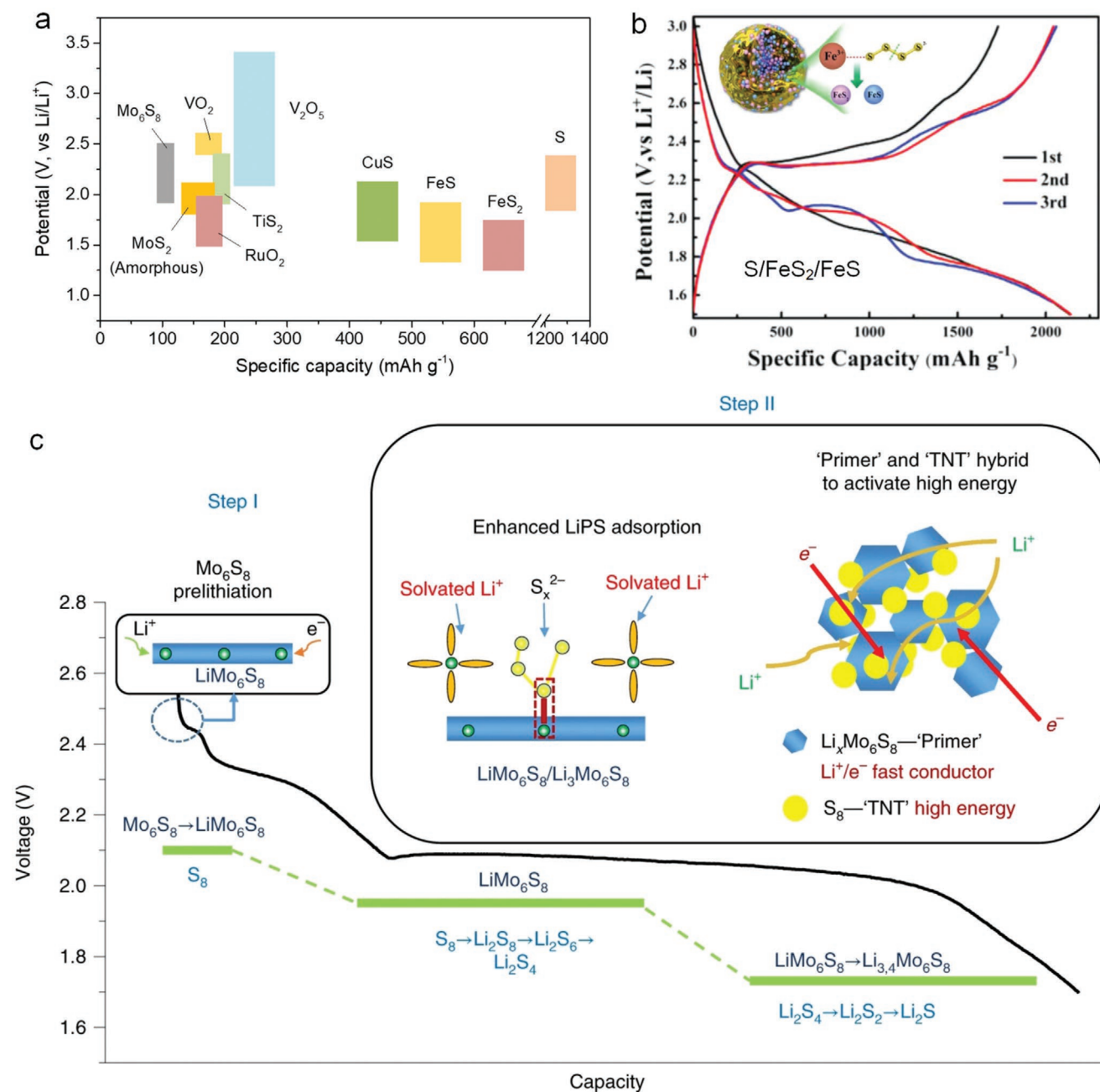


Figure 7. Electrochemically active metal oxides/sulfides for enhancing W_V . a) Potential (vs Li/Li⁺) versus specific capacity of several active metal oxides and sulfides: Mo₆S₈,^[32b] amorphous MoS₂,^[93] VO₂,^[94] V₂O₅,^[95] TiS₂,^[92b,96] RuO₂,^[97] FeS,^[98] FeS₂,^[99] CuS.^[100] b) Discharge–charge curves of hybrid S/FeS₂/FeS composite in ether-based electrolyte. Reproduced with permission.^[32a] Copyright 2019, Wiley-VCH. c) Demonstration of sulfur/Mo₆S₈ hybrid cathode. The role of the Chevrel-phase Mo₆S₈ in the S₈/Mo₆S₈ cathode, including a prelithiation before sulfur reduction above 2.4 V (vs Li/Li⁺) in step I, and a postlithiation in step II where the interaction between LiPS and LiMo₆S₈/Li₃Mo₆S₈ is formed and the intercalation reaction in Li_xMo₆S₈ provides a fast Li-ion transport channel for sulfur reduction. Reproduced with permission.^[32b] Copyright 2019, Springer Nature.

a mass density of 2 g cm⁻³_{cathode} that is close to that of the elemental sulfur (Figure 8d). The high energy densities of 1959 Wh L⁻¹_{cathode} and 980 Wh kg⁻¹_{cathode} are obtained based on cathode volume and mass, respectively. Recently, compact phosphorus-sulfur/graphene composite is reported to serve as flexible cathode (Figure 8e).^[105] At high temperature of 320 °C, phosphorus reacts with sulfur to form a phosphorus–sulfur

compound (P₂S_x), which is a clay-like material. After pressing to thin flakes of 30–45 μm, the phosphorus–sulfur/graphene cathode achieves a high density of 2.16 g cm⁻³_{cathode}, and the corresponding high energy densities of 3480 Wh L⁻¹_{cathode} and 1611 Wh kg⁻¹_{cathode} are achieved at low 0.06C rate and E/S ratio of 35 μL mg⁻¹. Although the advantage in enhancing W_V is impressive, the high W_G of the cell with sulfur-rich materials

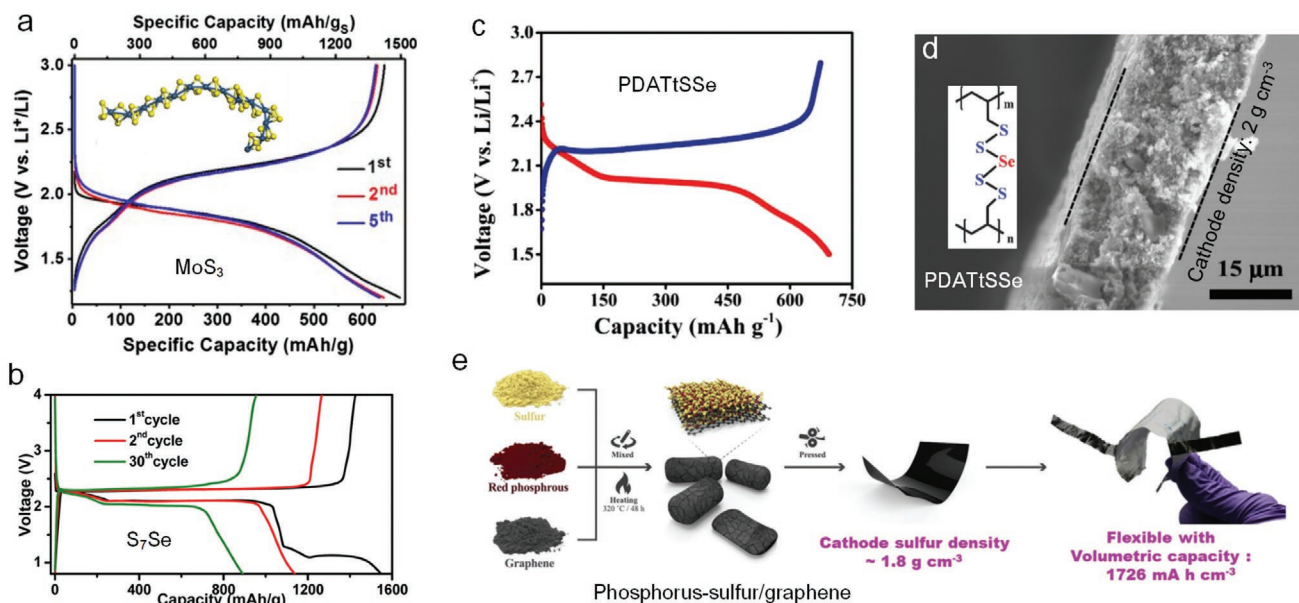


Figure 8. Sulfur-rich materials for high W_V . a) Voltage profiles of MoS₃ cathode in ether-based electrolyte. Reproduced with permission.^[106a] Copyright 2017, National Academy of Sciences. b) Voltage profiles of S₇Se cathode in ether-based electrolyte. Reproduced with permission.^[103a] Copyright 2013, American Chemical Society. c,d) Selenium-doped poly(diallyl terasulfide) (PDATtSSe) as cathodes for lithium-organosulfur battery: c) Voltage profiles of PDATtSSe in ether-based electrolyte and d) SEM image of compact cathode (PDATtSSe loading: 5.1 mg cm⁻²). Reproduced with permission.^[56] Copyright 2017, Wiley-VCH. e) Schematic illustration showing the preparation of compact phosphorus-sulfur/graphene cathodes with high volumetric capacity. Reproduced with permission.^[105] Copyright 2020, Elsevier.

should be initially guaranteed. As shown in Table S19 (Supporting Information), the sulfur content in sulfur-rich materials is generally limited within 80 wt%. Assuming a complete conversion of sulfur to lithium sulfide, the theoretical capacities of MoS₃ and PDATtSSe are only 837 and 742 mAh g⁻¹, respectively. Therefore, the optimization design of W_V and W_G should be considered preferentially for practical application.

3.2. Li-S Coin Cells with Freestanding Sulfur Cathode

Different from slurry cast cathode made by powders and current collector, the freestanding cathode is constructed by utilizing CNTs, graphene, carbon nanofibers (CNF), or other carbon materials as conductive scaffold without the binder and current collector.^[27b,30a,112] High sulfur loading (>10 mg cm⁻²) and high areal capacity (>10 mAh cm⁻²) can be easily achieved through freestanding cathode, thus giving rise to a really high W_G . As shown in Table 4, 1000 Wh kg⁻¹_{cathode} of W_G is an easy target for the most of the reported freestanding cathodes. However, 1000 Wh L⁻¹_{cathode} of W_V is a difficult goal to achieve for the freestanding cathode, because of the porous carbon matrix and low density (≈ 0.5 g cm⁻³).^[112a,113] Indeed, increasing the sulfur fraction is an effective way to improve the density for freestanding cathode. For example, with carbon fibers as freestanding scaffold, the cathode density is raised from 0.68 to 1.4 g cm⁻³_{cathode} when sulfur fraction is increased from 57 to 73 wt%.^[114] When carbon cotton with hierarchical macro-/microporous architectures is used as ideal conductive matrix, the areal sulfur loading can reach a superhigh value of 576 mg cm⁻².^[113b,c,115] At the sulfur loading of 30.7 mg cm⁻²,

the cathode delivers a high areal capacity of 36 mAh cm⁻², corresponding to high W_V and W_G of 2522 Wh L⁻¹_{cathode} and 1971 Wh kg⁻¹_{cathode}, respectively.^[115e]

Introducing compact carbon/carbon-free hosts or designing a closely packed structure can transform the loose freestanding cathode to a compact one.^[115b,116] A good demonstration is shown in the closely stacked self-standing conductive scaffold as host, in which CNTs penetrate throughout the MOF-derived porous carbon polyhedrons.^[116b] At sulfur fraction of 70 wt% and sulfur loading of 6.4 mg cm⁻², the cathode has a high density of 1.47 g cm⁻³_{cathode} and corresponding W_V of 1743 Wh L⁻¹_{cathode} at 0.2C rate. When the carbon polyhedrons are replaced with MOF crystals, the freestanding cathode achieves a higher density of 2.18 g cm⁻³_{cathode} and W_V of 2509 Wh L⁻¹_{cathode}.^[116d] Recently, a carbon-free freestanding cathode using graphene-like RuO₂ as conductive scaffold is reported.^[91] The cathode consists of 65.5 wt% sulfur and 34.5 wt% RuO₂, where RuO₂ serves not only as efficient host, but also as active materials (theoretical specific capacity 201 mAh g⁻¹) to contribute additional capacity. At the high sulfur loading of 8.4 mg cm⁻², the S/RuO₂ freestanding cathode has a really high density of 2.95 g cm⁻³_{cathode} and high W_V of 4160 Wh L⁻¹_{cathode}.

3.3. Li-S Pouch Cells

The evaluation on Li-S pouch cells is closer to practical application than coin cells. Figure 9a-e shows the typical components of a Li-S pouch cell, including S/C composites, coated cathode, lithium foil, double side cathode, and prismatic pouch cell. As mentioned in Introduction, W_V of Li-S battery is unsatisfactory

Table 4. Gravimetric/volumetric energy density of freestanding sulfur cathodes and corresponding full Li–S cells.

Sulfur host	C-rate	Areal loading [mg cm ⁻²]	Sulfur fraction [wt%]	Areal capacity [mAh cm ⁻²]	Cathode density [g cm ⁻³]	Cathode thickness [μm]	Voltage/ [V]	Cathode ^{a)}		E/S/ [μL mg ⁻¹]	Cell ^{b)}		Ref.
								W _V [Wh L ⁻¹]	W _G [Wh kg ⁻¹]		W _V [Wh L ⁻¹]	W _G [Wh kg ⁻¹]	
Graphene/CNT	0.2C	2.5	77.8	2.67	0.23	140	2.1	401	1743	15	277.5	348	[113a]
CNT	0.05C	6.3	54	6.2	0.47	250	2.1	527	1128	9.6	401	393	[112a]
CNF	0.05C	18.1	55	19.5	0.56	588	2.1	704	1247	14	484	437	[113b]
Carbon paper	0.05C	30	68.8	20.2	0.93	470	2.1	904	972	10	804	484	[115a]
Carbon sphere/ graphene	0.2C	3.9	62	5.3	0.524	120	2.1	928	1771	—	460	377	[113c]
Graphene/CNT	0.05C	4.7	53	~5.41	1.27	70	2.1	1626	1280	9.6	728	373	[30a]
Carbon spheres/ MWCNT	0.05C	5	54	6.1	1.68	55	2.1	2317	1379	6	848	379	[116c]
Carbon cotton	0.1C	30.7	80	36	1.28	300	2.1	2522	1971	6.8	1037	508	[115e]
CNF	0.2C	3.9	72.3	4.29	0.69	78	2.0	1098	1591	—	602	394	[27b]
Carbon-cotton	0.1C	57.6	75	31.33	1.28	600	2.1	1098	857	4.2	1019	507	[115d]
Carbon polyhedrons/CNT	0.2C	6.4	70	5.13	1.47	62	2.1	1743	1178	—	928	428	[116b]
CNF	0.1C	2.32	65.7	3.79	1.26	36	2.1	2212	1751	7.4	692	333	[112d]
Carbon fiber	0.05C	10.8	67	14.6	1.0	160	2.1	1902	1902	4.9	790	450	[114]
Graphene/carbon	0.1C	5	73	5.7	1.59	43	2.1	2793	1748	15	939	416	[112b]
Carbon nanotubes	0.1C	19.1	79	19.8	1.38	175	2.1	2379	1724	—	1047	495	[117]
Carbon nanofiber	0.05C	14.3	85	13.7	1.46	115	2.1	2501	1710	8	1089	496	[118]
TiO ₂ /Graphene	0.2C	3.2	62	4.06	0.86	60	2.1	1422	1654	9.3	605	360	[115b]
CNF/TiO ₂	0.5C	2	40	3.21	0.55	90	2.1	742	1349	—	299	266	[113d]
Graphene- PEDOT:PSS	0.2C	2	56.4	2.45	1.83	19.5	2.1	2648	1451	—	610	293	[116a]
CNF/Co ₃ S ₄	0.3C	7.5	55	7.1	0.85	160	2.1	933	1097	—	620	405	[119]
MOF/CNT	0.2C	4.57	70	3.59	2.18	30	2.1	2509	1146	10.9	1016	404	[116d]
Active RuO ₂ (34.5 wt%)	0.2C	8.4	65.5	9.3	2.46	52	2.1	3755	1526	12	1337	481	[91]
Phosphorus–sulfur	0.06C	5.4	80	5.2	2.25	30	2.1	3625	1611	35	1104	432	[105]

^{a)}Without considering the current collector. The data are collected or derived from literatures; ^{b)}Renormalized energy densities based on full cell for better comparison. The model in the full cell configuration is used in Figure 2b. N/P ratio is set to be 2 for areal sulfur loading exceeding 3 mg cm⁻², and lithium foil of 30 μm is used for sulfur loading below 3 mg cm⁻². To simulate the practical pouch cell, the E/S ratio of 2 μL mg⁻¹ is assumed. Since the influence of lean electrolyte on W_V is limited (as shown in Figure 3d), only cathode parameters are used for the calculation of W_V, including the areal sulfur loading, sulfur fraction and cathode density according to Equation (1). For the calculation of W_G, two cathode parameters (areal sulfur loading and sulfur fraction) and one electrolyte parameter (E/S ratio) are involved according to Equation (6).

by using the conventional carbon nanomaterials as host for sulfur cathode. Li group evaluated the effect of various cell parameters on energy densities and assembled a pouch Li–S cell using a lithium anode (200% excess) and a typical sulfur/carbon cathode that has a sulfur loading of 4.5–6.5 mg cm⁻², sulfur mass fraction of 75% and electrode porosity of 71–76%.^[20] The resultant W_V of the pouch cell is ≈300 Wh L⁻¹_{cell}, roughly half that of Li-ion batteries (700 Wh L⁻¹). To make W_V higher, as previously discussed in Section 3.1.2., heavy Mo₆S₈ is introduced to fabricate a hybrid sulfur/Mo₆S₈ cathode with a moderate porosity of ≈55%.^[32b] The assembled 1 Ah-level Li|sulfur/Mo₆S₈ pouch cell, using multilayer sulfur/Mo₆S₈ cathodes and lithium metal anodes (≈200% excess Li), delivers initial W_V and W_G of 366 Wh kg⁻¹_{cell} and 581 Wh L⁻¹_{cell}, based on cell

mass and volume, respectively (Figure 9f). Further, it is pointed out that the energy densities can be improved by optimizing the mass production of sulfur/Mo₆S₈ material and mechanical parameters of the pouch cell. For instance, W_V and W_G are predicted to reach 405 Wh kg⁻¹_{cell} and 712 Wh L⁻¹_{cell} if less lithium (50% excess Li) is used.

Liu and Shao group developed a polymer gel as a soft media for Li-ion transportation and electrolyte wetting. The polymer gel serves as a swellable reservoir for retaining the electrolyte and soluble LiPS, enabling Li–S pouch cell to work under lean electrolyte of 3.3 μL mg⁻¹.^[16] The polymer gel is comprised of poly(ethylene oxide) (PEO) and lithium bis(trifluoromethanesulfonyl) imide (LiTFSI) (60:40 by weight). The cathode was composed of S/CNT composite, Super P as

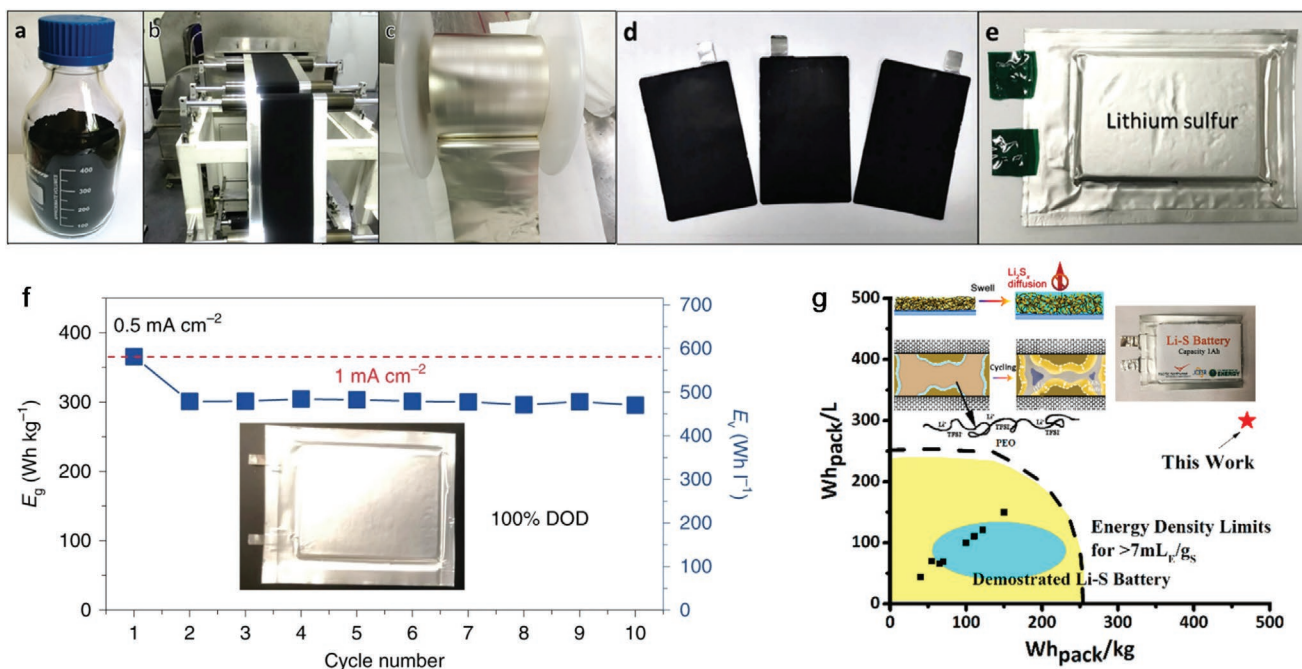


Figure 9. Digital photos of components of Li-S pouch cells: a) S/C composites; b) Coated cathode; c) Lithium metal foil; d) Double-side cathode; e) Prismatic Li-S pouch cell with a W_V of $\approx 300 \text{ Wh L}^{-1}$ (areal sulfur loading: $4.5\text{--}6.5 \text{ mg cm}^{-2}$, sulfur fraction: 75 wt%, cathode porosity: 71–76%, E/S ratio: $3 \mu\text{L mg}^{-1}$). Reproduced with permission.^[20] Copyright 2017, Elsevier. f) A 1 Ah Li-S pouch cell with sulfur/Mo₆S₈ cathode with an E/AM ratio of $1.2 \mu\text{L mg}^{-1}$. Reproduced with permission.^[32b] Copyright 2019, Springer Nature. g) Pouch Li-S cell with sulfur/MWCNT cathode and PEO-LiTFSI polymer gel (areal sulfur loading: 4 mg cm^{-2} , sulfur fraction: 64 wt%, cathode porosity: 65–70%, E/S ratio: $3.3 \mu\text{L mg}^{-1}$). Reproduced with permission.^[16] Copyright 2017, American Chemical Society.

conductive gent and PEO–LiTFSI as binder, with 64 wt% sulfur fraction, 4 mg cm^{-2} sulfur loading and 65–70% porosity. As shown in Figure 9g, the pouch cell had energy densities of $\approx 460 \text{ Wh kg}^{-1}$ and 300 Wh L^{-1} . These results are consistent with the discussion in Figure 2 that porous S/C cathode (density $\approx 0.6 \text{ g cm}^{-3}$, porosity $\approx 70\%$) cannot make higher W_V for Li-S battery. It is notable that higher W_V could be obtained if one takes no account of the cycling. For example, the primary Li-S battery, with a hierarchical porous S/C cathode of high sulfur loading of $6\text{--}14 \text{ mg cm}^{-2}$, could release energy densities of $504 \text{ Wh kg}^{-1}\text{-cell}$ and $654 \text{ Wh L}^{-1}\text{-cell}$ at 0.01 C, with excellent shelf stability for a month at room temperature.^[45] Of course, W_V of Li-S battery with the conventional S/C cathode is still unsatisfactory at that moment. Tuning the cathode structure to higher density ($>0.9 \text{ g cm}^{-3}$) and lower porosity ($<56\%$) is critical to achieve a decent W_V . In this sense, heavy hosts (compact carbon and carbon-free materials) and sulfur-rich materials are promising strategies for the purpose, and more work is needed to verify the feasibility in Li-S pouch cells.

3.4. The Catalytic Activity for Host Material

For enhancing W_V , a “Three High” technical strategy is proposed recently in our publication:^[31b] 1) High sulfur fraction of above 80 wt% for the sulfur-based composite or above 65 wt% for the cathode, 2) High sulfur loading of above 4 mg cm^{-2} for thick cathode, and 3) High density for the host materials (heavy host) with good electrocatalytic activity (Figure 10a). In particular, the

electrochemical processes, including diffusion, adsorption, and charge-transfer reactions, occur on the surface of host materials, so that the electrocatalytic activity of host is the key factor for ensuring fast redox of sulfur species and unlocking the high capacity release for the cell (Figure 10). Owing to the heavy and catalytic feature of host materials, a balance between densification and electroactivity can be achieved with respect to the sulfur cathode, which is essential to obtain high W_V and W_G simultaneously. In addition, the densified structure helps to reduce the cathode porosity and therefore lowers the electrolyte quantity, which in turn helps to improve W_G .

As discussed in Section 2.2, electrolyte quantity has a big impact on full Li-S cells, especially on W_G . In most cases (e.g., S/CNT cathode), the redox kinetics of sulfur species become considerably sluggish under lean electrolyte (ether-based system) because of the high viscosity and low ionic conductivity,^[41] which cause large cell polarization, low sulfur utilization, premature Li₂S passivation, and poor cycling performance.^[31a,b,41d,120] Therefore, the catalytic activity of host materials is very important in triggering the fast conversion of sulfur in lean electrolyte, enabling high capacity output with low polarization (Figure 10b).^[121] In this sense, the host materials are critical in dominating both W_V and W_G for Li-S battery. Thus, the “Three High” strategy can be further extended to a “Three High One Low (THOL)” strategy (high sulfur fraction, high sulfur loading, high density host with catalytic activity, and low electrolyte quantity) for both high W_V and W_G (Figure 10a).

A class of catalytic materials is reported in literatures, such as metal oxides,^[31a,b,73,82,122] sulfides,^[74–76,123] phosphides,^[121a,124]

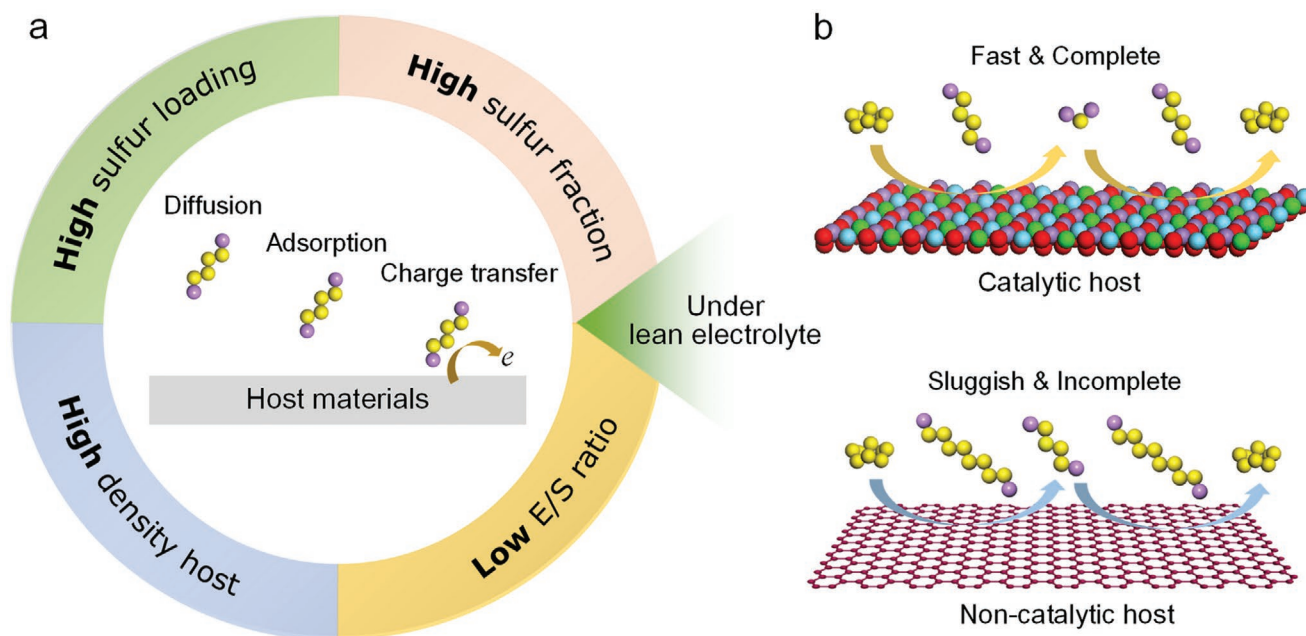


Figure 10. The significance of catalytic hosts in Li-S battery. a) The “Three High One Low (THOL)” strategy for achieving a balance of W_V and W_G , where the catalytic hosts play important roles not only in densifying the electrode, but also in accelerating the reaction kinetics under lean electrolyte. The inset shows the diffusion, adsorption, and charge-transfer processes of sulfur species on the surface of host materials. b) Schematic illustration of fast and complete conversion of sulfur species on catalytic hosts, and sluggish and incomplete conversion of sulfur species on noncatalytic hosts under lean electrolyte condition.

nitrides,^[78,125] carbides,^[58,126] Co,^[81] Pt,^[80] C₃N₄,^[127] heteroatom-doped carbon,^[128] and black phosphorus quantum dots.^[129] Polar catalytic hosts in many cases can effectively absorb dissolved polysulfides by forming strong polar-polar interactions or weak metal-sulfur bonding, thereby alleviating the shuttle effect and prolonging the battery life.^[130] Despite the enhanced kinetics, catalytic hosts are generally electrochemically inert and unavoidably take up extra weight and volume, which goes against the energy densities. Hence, the fraction of catalyst materials needs to be controlled as low as possible on the premise of ensuring the catalytic effect. According to the analysis in Section 2.2, 70 wt% sulfur in cathode is indispensable in terms of both W_V and W_G . Taking into account the conductive agent (5–10 wt%) and binder (5–10 wt%), the mass percentage of catalytic hosts should be less than 10–20 wt%. To decrease the volume of inactive hosts, higher density is preferred, just as indicated in Figure 2. In addition, high specific area of catalytic host is also required in order to provide enough active sites to catalyze the reaction of sulfur species.

4. Electrode Engineering Technologies for Enhancing W_V

4.1. The Calendering Technology

Calendering is a typical engineering process that is indispensable for the production of Li-ion batteries. On one hand, calendering can improve the adhesion between electrode material and current collector. On the other hand, calendering can increase compaction density of electrodes by enhancing the

particle-to-particle contact, which not only reduces the ohmic resistance but also leads to lower porosity and greater W_V . However, due to the intrinsic dissolution-deposition mechanism of sulfur, things become rather complex when sulfur cathode is subjected to a calendering operation.

In a simple description, the degree of calendering is expressed in the compaction ratio, which is defined as the ratio of thickness variation to the initial thickness of cathode.^[30a] By taking freestanding S/CNT/graphene cathode as an example, the mechanical properties of electrode, such as strength and elongation, can be enhanced by moderate calendering, and the ohmic resistance is reduced with compaction ratio owing to the enhanced contact between CNT and graphene.^[30a] Moreover, the electrode porosity declines dramatically under calendering, especially for the vulnerable macropores. This leads to a remarkable decrease of electrolyte uptake. When the compaction ratio is increased from 0 to 60.6%, the cathode density is increased from 0.25 to 1.27 g cm⁻³_{cathode}, along with the W_V enhancement from 275 to 853 Wh L⁻¹_{cathode} (Figure 11a).

However, calendering has more complicated impacts on slurry cast sulfur cathode. For the S/La_{0.8}Sr_{0.2}MnO₃ cathode, after pressing at a mild pressure of ≈0.2 MPa, the cathode density is remarkably increased from 0.98 to 1.69 g cm⁻³_{cathode}, together with the porosity decrease from 55 to 21% (Figure 11b).^[31b] Comparing with the bare cathode, the pressed cathode shows a big W_V advance from 1787 to 2727 Wh L⁻¹_{cathode} at the sulfur loading of 6.2 mg cm⁻² and E/S ratio of 7 μL mg⁻¹. Of course, some problems arise from further increasing pressure, such as the lower discharge voltage and reduced capacity output caused by poor electrolyte wetting in the low porosity. As a direct result, despite the improved W_V , the W_G shows a slight decrease from

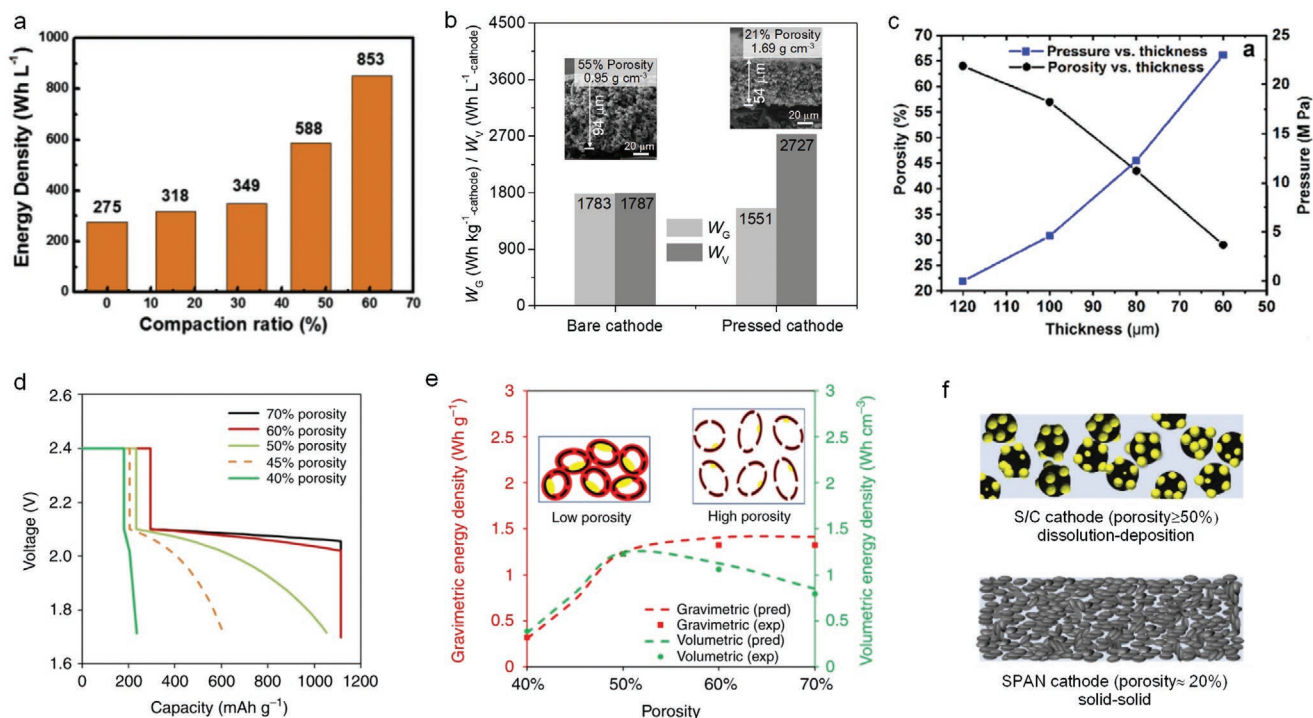


Figure 11. Influence of calendaring on sulfur cathode. a) Freestanding cathode: dependence of W_V on compaction ratio. Reproduced with permission.^[30a] Copyright 2017, Elsevier. b–f) Slurry cast cathode: b) Comparison of W_V and W_G between the bare and pressed $S/La_{0.8}Sr_{0.2}MnO_3$ cathodes. The inset shows the SEM images of cross section of bare and pressed cathodes, and the porosity and density are also indicated. Reproduced with permission.^[31b] Copyright 2020, Wiley-VCH. c) The relationship between electrode porosity, thickness, and calendaring pressure. Reproduced with permission.^[30b] Copyright 2018, American Chemical Society. d) Schematic of discharge curves for sulfur cathodes of different porosities. e) Predicted W_V and W_G based on the total mass of sulfur cathode including sulfur, host, conductive agent, and binder without current collector. In the inset, the yellow, black, and red stand for the unutilized sulfur, carbon matrix, and deposited Li_2S_2/Li_2S , respectively. Reproduced with permission.^[39a] Copyright 2019, Springer Nature. f) Comparison of conventional S/C cathode and SPAN cathode. The porosity for the former is required to be higher than 50% due to the dissolution–deposition mechanism of sulfur, while the porosity for the latter could be reduced to 20% owing to the solid–solid conversion of sulfur. Reproduced with permission.^[63] Copyright 2020, Elsevier.

1783 to 1551 Wh kg⁻¹-cathode. The negative effect becomes more severe if higher pressure (over 0.5 MPa) is used. In addition, the minimum electrolyte quantity is decreased from 5 μL mg⁻¹ for bare cathode (55% porosity) to 4 μL mg⁻¹ for the pressed cathode (21% porosity) in coin cells, agreeing well with the discussion in Figure 3a. It implies that the pressed technology of electrode needs to be further optimized in order to get a balance between cathode density and electrochemical activity, especially under lean electrolyte conditions. Similar phenomena are also found for the typical S/C slurry cast cathode, as demonstrated by Zhang and Xiao Group.^[30b,49] As shown in Figure 11c, the thickness and porosity of the sulfur/carbon cathode decreases significantly with increasing calendaring pressure, benefiting the W_V for Li–S battery and also reducing the electrolyte quantity. For the cathode with 4 mg cm⁻² sulfur loading, when the calendaring pressure increases from 4.6 to 23 MPa, the porosity decreases from 64% to 29% and the W_V increases markedly from 650 to 1300 Wh L⁻¹-cathode.^[30b] However, a large pressure (>9 MPa) would block the continuous diffusion pathway of electrolyte within the highly compact cathode, which not only stops electrolyte from fully wetting electrode, but also decreases the ionic conductivity within the electrode.^[49]

To better understand the effect of the electrode porosity on sulfur conversion, Cai and Qi group developed an analytical

model based on the dissolution/deposition mechanism of sulfur and by assuming that LiPS only dissolves into the electrolyte of the pore within the electrode.^[39a] In this model, the first voltage plateau ($S_8 \rightarrow Li_2S_4$) is governed by the Li_2S_4 concentration dissolved in the electrolyte, and the second voltage plateau ($Li_2S_4 \rightarrow Li_2S_2/Li_2S$) is dominated by the electronically accessible surface area of the carbon matrix. The predicted discharge curves at different porosities are illustrated in Figure 11d. As the electrode porosity decreases, the concentration of Li_2S_4 increases, and capacity drop in the first voltage plateau region appears once the concentration reaches the saturation limit. In the meantime, the decrease of the effective surface area for Li_2S_2/Li_2S deposition results in the formation of thick insulation layer, leading to sharp voltage drop and voltage plateau shrinkage. The estimated W_V and W_G at different porosities are shown in Figure 11e, suggesting that a Li–S cell could achieve a maximum energy density at the cathode porosity of 52%. This model agrees with their experimental data and both of them indicate that the cathode cannot work at porosity below 40% due to the disappearance of the second voltage plateau (Figure 11d). The low porosity has an adverse effect on sulfur conversion as elucidated in theoretical analysis. Normally, the sulfur cathodes with the porosity of 20–30% can work at low current density, though the cell shows a relatively large polarization.^[30b,31b] In

that case, the catalytic host materials should be introduced to take action by accelerating the sulfur conversion under lean electrolyte, where LiPS concentration reaches saturation.^[31b,121a]

Interestingly, low porosity is more suitable for the solid–solid conversion of sulfur cathode in carbonate-based electrolyte, such as SPAN cathode. Wang group pointed out that suitable pressure is favorable to the battery performance owing to the better contact between SPAN cathode materials and current collector, as well as the enhanced electronic conductivity.^[63] At high pressure of 25 MPa, the density of SPAN cathode reaches to 1.54 g cm^{-3} with a really low porosity of 13.3%, similar to that of metal oxide cathode in Li-ion batteries. Impressively, the densified SPAN cathode shows only slight capacity loss and maintains a good electrochemical performance in carbonate-based electrolyte, with W_V and W_G of 1528 Wh L^{-1} and 992 Wh kg^{-1} , respectively. The less dependence of sulfur redox on cathode porosity is attributed to the solid–solid conversion mechanism of sulfur cathode in carbonate-based electrolyte without the formation of soluble LiPS (Figure 11f).

4.2. Dry Coating Technology of Electrode

Dry coating, or solvent-free coating, is a novel technology for preparing electrodes, which was invented in the early 2000s,^[131] and now is ready to manufacture in Li-ion batteries at Maxwell Technologies,^[132] an ultracapacitor manufacture in San Diego. This technology generally includes three stages: 1) Dry powder mixing/shearing of active materials, conductive carbon and polymer binder; 2) Dry-spraying or hot rolling to form a dry electrode film; 3) Attaching electrode film to current collector by hot pressing.^[132,133] Different from the slurry cast electrode, this technology avoids dissolving binder in organic solvent and thus results in a unique electrode structure. In particular, the binder network in electrode allows for high ionic conductivity and intimate contact between active materials and conductive carbon. Therefore, dry coating electrodes could achieve good cycling stability and excellent rate capability.

The feasibility of dry coating technology in Li–S battery has been verified by Maxwell Technologies and Kaskel et al.^[132,134] In Kaskel's work, the mechanically stable cathode film (53 wt% sulfur) is produced by rolling the well mixed and sheared mixture of sulfur-based composite, CNT, and poly(tetrafluoroethylene) at $150 \text{ }^\circ\text{C}$, which is then laminated onto the carbon-coated Al foil.^[134] The $80 \text{ }\mu\text{m}$ thickness yields a sulfur loading of $3.0\text{--}3.2 \text{ g cm}^{-2}$ for the cathode without considering Al foil. Compared with conventional slurry coating, this dry coating technology enables a higher cathode density of 0.755 g cm^{-3} , which corresponds to a porosity of $\approx 65\%$. Notably, the dry-coating cathode exhibits a good electroactivity, and delivers a maximum capacity of 1045 mAh g^{-1} and maintains 742 mAh g^{-1} after 160 cycles.^[134] The density and porosity can be further tuned by adjusting the sulfur fraction and the rolling process in order to achieve more compact sulfur cathodes. It is expected that, with the dry-coating technology, sulfur cathode may achieve a better balance between high density and good redox kinetics of sulfur, which needs more exploration in future researches. Other than the density advantage, another merit of dry coating is that the binder quantity in

electrode can be largely reduced. The minimum percentage of binder in Li-ion batteries is reported to be as low as 0.1 wt%.^[135] This one the one hand improves the cathode density by reducing the light-weight binder, and on the other hand allows for further increase of active sulfur in cathode, both of which benefit the cell energy densities.

5. Summary and Future Prospects

The energy density is the driving force for the development of secondary batteries. The past decades have witnessed the rapid development of high energy Li–S battery. The milestone on Li–S battery is the introduction of carbon micro/nanomaterials as sulfur host into cathode for improving the cycle stability. In the subsequent decade, a variety of carbon nanomaterials, including CNTs, graphene and hierarchical mesoporous carbon, brings new blood and fresh air to Li–S battery for enhancing W_G . All the performance evaluations based on sulfur/carbon composites as active materials are mainly focused on the gravimetric capacity and cycle stability of sulfur cathode, as well as W_G of Li–S battery. However, W_V is more important than W_G for mobile application within a confined space. As high energy battery system, W_V of Li–S battery is certainly brought into focus in more recent years, and ought to be paid more attention in future researches.

Typically, in Li–S battery, the key factors of dominating W_V are the sulfur content (areal loading and mass fraction), density/porosity of sulfur cathode and the electrolyte quantity. In order to achieve decent W_V target (700 Wh L^{-1}), sulfur cathode must meet the requirements of areal sulfur loading of $\approx 6 \text{ mg cm}^{-2}$, sulfur fraction of $\approx 70 \text{ wt}\%$, cathode density of $\approx 1.2 \text{ g cm}^{-3}$, porosity of less than 42%, and E/S ratio of $1 \text{ }\mu\text{L mg}^{-1}$. Among these requirements, cathode density is one of the biggest challenges because of the low density of active sulfur. Under the premise of high sulfur content for ensuring high W_G , there are generally three strategies to increase the cathode density: 1) Introducing compact carbon or heavy carbon-free hosts, such as metal oxides or sulfides. The electrocatalytic activity of host material is a critical factor to accelerate effective conversion of sulfur and to increase utilization of sulfur under lean electrolyte for enhancing both W_V and W_G . 2) Replacing sulfur with heavy sulfur-rich materials, for example selenium–sulfur solid solution or metal polysulfides. 3) Freestanding sulfur cathode to provide really high W_V and W_G for Li–S battery. All these strategies in Li–S coin cells must be further verified in Li–S pouch cells, including the enlargement of electrode manufacture and the optimization of electrolyte quantity.

Electrode engineering technology is the effective way to manipulate the electrode structure and porosity. By employing calendaring technology, the cathode density, and corresponding volumetric capacity can be raised. However, the densified structure with low porosity, which causes large polarization and low sulfur utilization, is unfavorable for the electrolyte penetration and the dissolution/deposition reactions of sulfur active materials. Therefore, the electrode engineering technology discussed here is to ensure the high density of the sulfur cathode, and simultaneously leave sufficient diffusion channels. At present, the electrode engineering technology for fabricating the sulfur

cathode is borrowed from conventional Li-ion battery technology, which was already demonstrated to be cheaper in battery production. In addition, cheap carbon-free host materials or sulfur-rich materials should be also considered based on the requirement of battery cost.

Lean electrolyte is indispensable for achieving high energy of Li-S battery. To reach $700 \text{ Wh L}^{-1}/500 \text{ Wh kg}^{-1}$, the E/S ratio in ether-based electrolyte must be decreased to $1 \mu\text{L mg}^{-1}$ in pouch cells. Under lean electrolyte, the high electrolyte viscosity, low sulfur utilization, and sluggish electrode kinetics appear consequently. Theoretically, all the problems under lean electrolyte are originated from the dissolution/deposition mechanism of active sulfur in ether-based electrolyte. Incorporating electrocatalysts into cathode or adding mediators into electrolyte could help to improve the reaction kinetics and promote the sulfur conversion. In particular, searching for new electrolyte beyond ether-based electrolyte potentially provides feasible solution. Sparingly solvating electrolyte, such as concentrated electrolyte, fluorinated electrolyte, or gel electrolyte, enables a low solubility of polysulfides and can fundamentally transform the sulfur reaction from dissolution/deposition to quasi-solid or solid conversion.^[136] This decouples the electrolyte quantity from sulfur mass and reaction mechanism, which makes it possible to operate Li-S battery under lean electrolyte. The limited dissolution of polysulfides also helps to construct a shuttle-free battery. Of course, the high viscosity and low ionic conductivity in sparingly solvating electrolyte are still faced in the coming studies. In addition, the combination of efficient electrocatalysts and sparingly solvating electrolyte is expected to achieve a decent reaction kinetics under lean electrolyte, which helps to improve both energy density and cycle life.

The rate capability is highly important for the battery application, which needs to be carefully evaluated for Li-S battery. Based on the dissolution/deposition mechanism, the current density for the thick sulfur cathode ($>4 \text{ mg cm}^{-2}$) is usually limited within 1 C rate, which is further decreased to below 0.5 C under lean electrolyte. As to the compact cathode, the densified electrode structure is likely to hinder the mass transfer due to the blocked inner channel, further depressing the rate capability. To address this challenge, a synergic and rational design of both cathode structure and electrolyte quantity should be required. First, as mentioned above, the porous electrode structure must be precisely regulated to provide sufficient channels for the electrolyte wetting/penetration and mass transfer of polysulfides. The cathode structure should also possess a good conductive skeleton in order to ensure the electron transport. Second, the ionic conductivity and electrolyte viscosity need to be optimized to ensure the fast mass transfer under lean electrolyte, which relies on either the modification of conventional ether-based electrolyte or the development of new electrolyte systems. Specifically, adding ammonium additives (NH_4NO_3 and NH_4I) or lithium salts with high donor number (DN) anions (LiNO_3 and LiBr) increases the solubility of Li_2S .^[137] This prevents the premature passivation and blocking of Li_2S on the cathode structure and benefits the high-rate capability.

In general, the capacity is controlled by cathode, while the cycle life is dominated mainly by anode for battery system. On the cathode side, the "Three High One Low (THOL)" strategy (high sulfur fraction, high sulfur loading, high density host,

and low electrolyte quantity) is appropriate for evaluation of the gravimetric/volumetric capacities of sulfur cathode in coin cells and pouch cells. On the anode side, the lithium anode technology should be taken more seriously for stabilizing the cycle performance of Li-S battery, including surface modification and lithium-alloying. In the industrialization transfer process from coin cells to pouch cells, the engineering technologies are key for manipulating desired density/porosity of the sulfur cathode, as well as the stabilization technology of anode. The battery design is also important for both W_V and W_G , including capacity matching, electrolyte optimization, separator modification, and quasisolid state design. More importantly, interdisciplinary technologies should be introduced into battery system to face the complexity on the reaction mechanism, key materials, and electrode structure, in order to boost W_V , W_G , and cycle life of Li-S battery. We have no doubt that the higher peaks on W_V and W_G of Li-S battery would be conquered in the future.

Supporting Information

Supporting Information is available from the Wiley Online Library or from the author.

Acknowledgements

Financial support from the National Key Research and Development Program (No. 2016YFB0100200), and National Natural Science Foundation (Nos. 21935006 and 21421001) of China is gratefully acknowledged.

Conflict of Interest

The authors declare no conflict of interest.

Keywords

electrocatalytic activity, host materials, lithium-sulfur batteries, sulfur cathodes, volumetric energy density

Received: June 9, 2020
Revised: September 18, 2020
Published online:

- [1] J. W. Choi, D. Aurbach, *Nat. Rev. Mater.* **2016**, *1*, 16013.
- [2] a) X. P. Gao, H. X. Yang, *Energy Environ. Sci.* **2010**, *3*, 174; b) Y. Yang, G. Y. Zheng, Y. Cui, *Chem. Soc. Rev.* **2013**, *42*, 3018.
- [3] a) H. Danuta, U. Juliusz, (Electric Techniques Corporation), *U.S. 3043896*, **1962**; b) M. L. B. Rao, (P. R. Mallory & Co., Inc.), *U.S. 3413154*, **1968**.
- [4] a) M. V. Merritt, D. T. Sawyer, *Inorg. Chem.* **1970**, *9*, 211; b) R. P. Martin, W. H. Doub, J. L. Roberts, D. T. Sawyer, *Inorg. Chem.* **1973**, *12*, 1921; c) R. D. Rauh, K. M. Abraham, G. F. Pearson, J. K. Surprenant, S. B. Brummer, *J. Electrochem. Soc.* **1979**, *126*, 523; d) E. Peled, Y. Sternberg, A. Gorenstein, Y. Lavi, *J. Electrochem. Soc.* **1989**, *136*, 1621.

- [5] a) J. Wang, J. Yang, J. Xie, N. Xu, *Adv. Mater.* **2002**, *14*, 963; b) Y. V. Mikhaylik, I. Kovalev, R. Schock, K. Kumaresan, J. Xu, J. Affinito, *ECS Trans.* **2010**, *25*, 23.
- [6] X. L. Ji, K. T. Lee, L. F. Nazar, *Nat. Mater.* **2009**, *8*, 500.
- [7] X. Y. Tao, J. G. Wang, C. Liu, H. T. Wang, H. B. Yao, G. Y. Zheng, Z. W. Seh, Q. X. Cai, W. Y. Li, G. M. Zhou, C. X. Zu, Y. Cui, *Nat. Commun.* **2016**, *7*, 11203.
- [8] S. Bai, X. Liu, K. Zhu, S. Wu, H. Zhou, *Nat. Energy* **2016**, *1*, 16094.
- [9] Q. Pang, A. Shyamsunder, B. Narayanan, C. Y. Kwok, L. A. Curtiss, L. F. Nazar, *Nat. Energy* **2018**, *3*, 783.
- [10] M. S. Kim, J.-H. Ryu, Y. R. L. Deepika, I. W. Nah, K.-R. Lee, L. A. Archer, W. Il Cho, *Nat. Energy* **2018**, *3*, 889.
- [11] a) J. S. Yeon, S. Yun, J. M. Park, H. S. Park, *ACS Nano* **2019**, *13*, 5163; b) M. Jana, R. Xu, X.-B. Cheng, J. S. Yeon, J. M. Park, J.-Q. Huang, Q. Zhang, H. S. Park, *Energy Environ. Sci.* **2020**, *13*, 1049; c) J. C. Guo, Y. H. Xu, C. S. Wang, *Nano Lett.* **2011**, *11*, 4288; d) G. Li, J. Sun, W. Hou, S. Jiang, Y. Huang, J. Geng, *Nat. Commun.* **2016**, *7*, 10601.
- [12] a) I. Kovalev, Y. Mikhaylik, T. T. Weiß, *High Energy Rechargeable Li-S Battery Development at Sion Power and Basf*, Li-S Workshop, Dresden **2013**; b) Sion Power's Lithium-Sulfur Batteries Power High Altitude Pseudo-Satellite Flight. <https://sionpower.com/2014/sion-powers-lithium-sulfur-batteries-power-high-altitude-pseudo-satellite-flight/> (accessed: August 2020).
- [13] Oxis Energy Is Close to Achieving 500wh/Kg and Is Targeting 600wh/Kg with Solid State Lithium Sulfur Technology. <https://oxisenergy.com/https-oxisenergy-com-wp-content-uploads-2020-01-500-and-600-whkg-pressor-pdf/> (accessed: August 2020).
- [14] a) Progress of Lithium-Sulfur Battery in Dalian Institute of Chemical Physics, Chinese Academy of Sciences. http://www.cas.cn/syky/201801/t20180115_4632252.shtml, (accessed: August 2020); b) W. Wang, A. Wang, Z. Jin, *Energy Storage Sci. Technol.* **2020**, *9*, 593.
- [15] Y. Mikhaylik, I. Kovalev, C. Scordilis-Kelley, L. Liao, M. Laramie, U. Schoop, T. Kelley, 650 Wh/Kg, 1400 Wh/L Rechargeable Batteries for New Era of Electrified Mobility, Sion Power, 2018 NASA Aerospace Battery Workshop, Huntsville, Alabama, USA **2018**.
- [16] J. Chen, W. A. Henderson, H. Pan, B. R. Perdue, R. Cao, J. Z. Hu, C. Wan, K. S. Han, K. T. Mueller, J.-G. Zhang, Y. Shao, J. Liu, *Nano Lett.* **2017**, *17*, 3061.
- [17] First-Generation Licerion Cell in Sion Power. <https://sionpower.com/news/> (accessed: August 2020).
- [18] a) M. Hagen, D. Hanselmann, K. Ahlbrecht, R. Maça, D. Gerber, J. Tübke, *Adv. Energy Mater.* **2015**, *5*, 1401986; b) B. D. McCloskey, *J. Phys. Chem. Lett.* **2015**, *6*, 4581.
- [19] Sion Power Announces Launch of Its Groundbreaking Licerion Rechargeable Lithium Battery. <https://sionpower.com/2018/sion-power-announces-launch-of-its-groundbreaking-licerion-rechargeable-lithium-battery/> (accessed: August 2020).
- [20] W. Xue, L. Miao, L. Qie, C. Wang, S. Li, J. Wang, J. Li, *Curr. Opin. Electrochem.* **2017**, *6*, 92.
- [21] C. Zhang, W. Lv, Y. Tao, Q.-H. Yang, *Energy Environ. Sci.* **2015**, *8*, 1390.
- [22] a) X. Feng, M. Ouyang, X. Liu, L. Lu, Y. Xia, X. He, *Energy Storage Mater.* **2018**, *10*, 246; b) O. Gröger, H. A. Gasteiger, J.-P. Suchsland, *J. Electrochem. Soc.* **2015**, *162*, A2605.
- [23] China's Catl Unveils Cell-to-Pack Battery Platform, https://www.xinhuanet.com/english/2019-09/13/c_138389934.htm (accessed: August 2020).
- [24] Oxis Energy: Revolutionizing Battery Technology with Lithium-Sulfur. <https://www.azom.com/article.aspx?ArticleID=19403> (accessed: August 2020).
- [25] J. Gao, H. D. Abuña, *J. Phys. Chem. Lett.* **2014**, *5*, 882.
- [26] X. B. Cheng, J. Q. Huang, Q. Zhang, H. J. Peng, M. Q. Zhao, F. Wei, *Nano Energy* **2014**, *4*, 65.
- [27] a) Y.-Z. Zhang, Z. Zhang, S. Liu, G.-R. Li, X.-P. Gao, *ACS Appl. Mater. Interfaces* **2018**, *10*, 8749; b) Z. Li, J. T. Zhang, Y. M. Chen, J. Li, X. W. Lou, *Nat. Commun.* **2015**, *6*, 8850.
- [28] T. Xu, J. Song, M. L. Gordin, H. Sohn, Z. Yu, S. Chen, D. Wang, *ACS Appl. Mater. Interfaces* **2013**, *5*, 11355.
- [29] a) Q. Pang, X. Liang, C. Y. Kwok, J. Kulisch, L. F. Nazar, *Adv. Energy Mater.* **2017**, *7*, 1601630; b) X. Yu, J. Deng, R. Lv, Z.-H. Huang, B. Li, F. Kang, *Energy Storage Mater.* **2019**, *20*, 14.
- [30] a) P.-Y. Zhai, J.-Q. Huang, L. Zhu, J.-L. Shi, W. Zhu, Q. Zhang, *Carbon* **2017**, *111*, 493; b) D. Lu, Q. Li, J. Liu, J. Zheng, Y. Wang, S. Ferrara, J. Xiao, J.-G. Zhang, J. Liu, *ACS Appl. Mater. Interfaces* **2018**, *10*, 23094.
- [31] a) Y. T. Liu, D. D. Han, L. Wang, G. R. Li, S. Liu, X. P. Gao, *Adv. Energy Mater.* **2019**, *9*, 1803477; b) Y. T. Liu, S. Liu, G. R. Li, X. P. Gao, *Adv. Sci.* **2020**, *7*, 1903693; c) Z. Xiao, Z. Yang, Z. Li, P. Li, R. Wang, *ACS Nano* **2019**, *13*, 3404; d) Q. Pang, D. Kundu, L. F. Nazar, *Mater. Horiz.* **2016**, *3*, 130.
- [32] a) K. Xi, D. He, C. Harris, Y. Wang, C. Lai, H. Li, P. R. Coxon, S. Ding, C. Wang, R. V. Kumar, *Adv. Sci.* **2019**, *6*, 1800815; b) W. Xue, Z. Shi, L. Suo, C. Wang, Z. Wang, H. Wang, K. P. So, A. Maurano, D. Yu, Y. Chen, L. Qie, Z. Zhu, G. Xu, J. Kong, J. Li, *Nat. Energy* **2019**, *4*, 374; c) L. Zhou, L. Yao, S. Li, J. Zai, S. Li, Q. He, K. He, X. Li, D. Wang, X. Qian, *J. Mater. Chem. A* **2019**, *7*, 3618.
- [33] Y. Cao, M. Li, J. Lu, J. Liu, K. Amine, *Nat. Nanotechnol.* **2019**, *14*, 200.
- [34] J. Betz, G. Bieker, P. Meister, T. Placke, M. Winter, R. Schmuch, *Adv. Energy Mater.* **2019**, *9*, 1803170.
- [35] a) S. Waluś, G. Offer, I. Hunt, Y. Patel, T. Stockley, J. Williams, R. Purkayastha, *Energy Storage Mater.* **2018**, *10*, 233; b) C. Weller, S. Thieme, P. Hartel, H. Althues, S. Kaskel, *J. Electrochem. Soc.* **2017**, *164*, A3766.
- [36] G. Gritzner, G. Kreysa, *J. Electroanal. Chem.* **1993**, *360*, 351.
- [37] Z. P. Cano, D. Banham, S. Ye, A. Hintennach, J. Lu, M. Fowler, Z. Chen, *Nat. Energy* **2018**, *3*, 279.
- [38] A. Jozwiuk, B. B. Berkes, T. Weiß, H. Sommer, J. Janek, T. Brezesinski, *Energy Environ. Sci.* **2016**, *9*, 2603.
- [39] a) N. Kang, Y. Lin, L. Yang, D. Lu, J. Xiao, Y. Qi, M. Cai, *Nat. Commun.* **2019**, *10*, 4597; b) C. Heubner, A. Nickol, J. Seeba, S. Reuber, N. Junker, M. Wolter, M. Schneider, A. Michaelis, *J. Power Sources* **2019**, *419*, 119.
- [40] a) J. Lochala, D. Liu, B. Wu, C. Robinson, J. Xiao, *ACS Appl. Mater. Interfaces* **2017**, *9*, 24407; b) G. Zhang, H.-J. Peng, C.-Z. Zhao, X. Chen, L.-D. Zhao, P. Li, J.-Q. Huang, Q. Zhang, *Angew. Chem., Int. Ed.* **2018**, *57*, 16732.
- [41] a) F. Y. Fan, Y.-M. Chiang, *J. Electrochem. Soc.* **2017**, *164*, A917; b) F. Y. Fan, M. S. Pan, K. C. Lau, R. S. Assary, W. H. Woodford, L. A. Curtiss, W. C. Carter, Y.-M. Chiang, *J. Electrochem. Soc.* **2016**, *163*, A3111; c) M. Zhao, B.-Q. Li, H.-J. Peng, H. Yuan, J.-Y. Wei, J.-Q. Huang, *Angew. Chem., Int. Ed.* **2020**, *59*, 12636; d) C. Shen, J. Xie, M. Zhang, P. Andrei, M. Hendrickson, E. J. Plichta, J. P. Zheng, *Electrochim. Acta* **2017**, *248*, 90.
- [42] C. Zhang, D.-H. Liu, W. Lv, D.-W. Wang, W. Wei, G.-M. Zhou, S. Wang, F. Li, B.-H. Li, F. Kang, Q.-H. Yang, *Nanoscale* **2015**, *7*, 5592.
- [43] K. R. Kim, K.-S. Lee, C.-Y. Ahn, S.-H. Yu, Y.-E. Sung, *Sci. Rep.* **2016**, *6*, 32433.
- [44] G. Babu, L. M. Reddy Arava, *RSC Adv.* **2015**, *5*, 47621.
- [45] Y. Ma, H. Zhang, B. Wu, M. Wang, X. Li, H. Zhang, *Sci. Rep.* **2015**, *5*, 14949.
- [46] C. Hu, C. Kirk, Q. Cai, C. Cuadrado-Collados, J. Silvestre-Albero, F. Rodríguez-Reinoso, M. J. Biggs, *Adv. Energy Mater.* **2017**, *7*, 1701082.
- [47] H. Li, Y. Tao, C. Zhang, D. Liu, J. Luo, W. Fan, Y. Xu, Y. Li, C. You, Z.-Z. Pan, M. Ye, Z. Chen, Z. Dong, D.-W. Wang, F. Kang, J. Lu, Q.-H. Yang, *Adv. Energy Mater.* **2018**, *8*, 1703438.

- [48] M. Li, Y. Zhang, F. Hassan, W. Ahn, X. Wang, W. W. Liu, G. Jiang, Z. Chen, *J. Mater. Chem. A* **2017**, *5*, 21435.
- [49] D. Lv, J. Zheng, Q. Li, X. Xie, S. Ferrara, Z. Nie, L. B. Mehdi, N. D. Browning, J.-G. Zhang, G. L. Graff, J. Liu, J. Xiao, *Adv. Energy Mater.* **2015**, *5*, 1402290.
- [50] F. Zeng, A. Wang, W. Wang, Z. Jin, Y.-S. Yang, *J. Mater. Chem. A* **2017**, *5*, 12879.
- [51] W. Li, Z. Liang, Z. Lu, H. Yao, Z. W. Seh, K. Yan, G. Zheng, Y. Cui, *Adv. Energy Mater.* **2015**, *5*, 1500211.
- [52] W. Li, G. Zheng, Y. Yang, Z. W. Seh, N. Liu, Y. Cui, *Proc. Natl. Acad. Sci. USA* **2013**, *110*, 7148.
- [53] Z. L. Li, Z. B. Xiao, S. Q. Wang, Z. B. Cheng, P. Y. Li, R. H. Wang, *Adv. Funct. Mater.* **2019**, *29*, 1902322.
- [54] X. Tao, J. Zhang, Y. Xia, H. Huang, J. Du, H. Xiao, W. Zhang, Y. Gan, *J. Mater. Chem. A* **2014**, *2*, 2290.
- [55] Y. Cao, X. Li, I. A. Aksay, J. Lemmon, Z. Nie, Z. Yang, J. Liu, *Phys. Chem. Chem. Phys.* **2011**, *13*, 7660.
- [56] J. Zhou, T. Qian, N. Xu, M. Wang, X. Ni, X. Liu, X. Shen, C. Yan, *Adv. Mater.* **2017**, *29*, 1701294.
- [57] Z. Cheng, Z. Xiao, H. Pan, S. Wang, R. Wang, *Adv. Energy Mater.* **2018**, *8*, 1702337.
- [58] Z. Xiao, Z. Li, P. Li, X. Meng, R. Wang, *ACS Nano* **2019**, *13*, 3608.
- [59] Q. Pang, L. F. Nazar, *ACS Nano* **2016**, *10*, 4111.
- [60] J. Zhang, H. Hu, Z. Li, X. W. Lou, *Angew. Chem., Int. Ed.* **2016**, *55*, 3982.
- [61] Z. Xiao, Z. Yang, L. Zhou, L. Zhang, R. Wang, *ACS Appl. Mater. Interfaces* **2017**, *9*, 18845.
- [62] L. Wang, Y.-H. Song, B.-H. Zhang, Y.-T. Liu, Z.-Y. Wang, G.-R. Li, S. Liu, X.-P. Gao, *ACS Appl. Mater. Interfaces* **2020**, *12*, 5909.
- [63] J. Chen, H. Zhang, H. Yang, J. Lei, A. Naveed, J. Yang, Y. Nuli, J. Wang, *Energy Storage Mater.* **2020**, *27*, 307.
- [64] B.-J. Lee, T.-H. Kang, H.-Y. Lee, J. S. Samdani, Y. Jung, C. Zhang, Z. Yu, G.-L. Xu, L. Cheng, S. Byun, Y. M. Lee, K. Amine, J.-S. Yu, *Adv. Energy Mater.* **2020**, *10*, 1903934.
- [65] a) J. X. Song, M. L. Gordin, T. Xu, S. R. Chen, Z. X. Yu, H. Sohn, J. Lu, Y. Ren, Y. H. Duan, D. H. Wang, *Angew. Chem., Int. Ed.* **2015**, *54*, 4325; b) H. Sohn, M. L. Gordin, M. Regula, D. H. Kim, Y. S. Jung, J. Song, D. Wang, *J. Power Sources* **2016**, *302*, 70.
- [66] H. Li, X. Yang, X. Wang, M. Liu, F. Ye, J. Wang, Y. Qiu, W. Li, Y. Zhang, *Nano Energy* **2015**, *12*, 468.
- [67] C. Zhang, Q.-H. Yang, *Sci. China Mater.* **2015**, *58*, 349.
- [68] M.-S. Song, S.-C. Han, H.-S. Kim, J.-H. Kim, K.-T. Kim, Y.-M. Kang, H.-J. Ahn, S. X. Dou, J.-Y. Lee, *J. Electrochem. Soc.* **2004**, *151*, A791.
- [69] Z. Wei Seh, W. Li, J. J. Cha, G. Zheng, Y. Yang, M. T. McDowell, P.-C. Hsu, Y. Cui, *Nat. Commun.* **2013**, *4*, 1331.
- [70] Z. Li, B. Y. Guan, J. T. Zhang, X. W. Lou, *Joule* **2017**, *1*, 576.
- [71] Q. Pang, D. Kundu, M. Cuisinier, L. F. Nazar, *Nat. Commun.* **2014**, *5*, 4759.
- [72] X. Liang, C. Hart, Q. Pang, A. Garsuch, T. Weiss, L. F. Nazar, *Nat. Commun.* **2015**, *6*, 5682.
- [73] L. B. Ma, R. P. Chen, G. Y. Zhu, Y. Hu, Y. R. Wang, T. Chen, J. Liu, Z. Jin, *ACS Nano* **2017**, *11*, 7274.
- [74] H. B. Lin, L. Q. Yang, X. Jiang, G. C. Li, T. R. Zhang, Q. F. Yao, G. W. Zheng, J. Y. Lee, *Energy Environ. Sci.* **2017**, *10*, 1476.
- [75] S. Wang, H. Chen, J. Liao, Q. Sun, F. Zhao, J. Luo, X. Lin, X. Niu, M. Wu, R. Li, X. Sun, *ACS Energy Lett.* **2019**, *4*, 755.
- [76] Z. Yuan, H. J. Peng, T. Z. Hou, J. Q. Huang, C. M. Chen, D. W. Wang, X. B. Cheng, F. Wei, Q. Zhang, *Nano Lett.* **2016**, *16*, 519.
- [77] Z. M. Cui, C. X. Zu, W. D. Zhou, A. Manthiram, J. B. Goodenough, *Adv. Mater.* **2016**, *28*, 6926.
- [78] D. R. Deng, F. Xue, Y. J. Jia, J. C. Ye, C. D. Bai, M. S. Zheng, Q. F. Dong, *ACS Nano* **2017**, *11*, 6031.
- [79] Q. Pang, C. Y. Kwok, D. Kundu, X. Liang, L. F. Nazar, *Joule* **2019**, *3*, 136.
- [80] H. Al Salem, G. Babu, C. V. Rao, L. M. R. Arava, *J. Am. Chem. Soc.* **2015**, *137*, 11542.
- [81] Z. Du, X. Chen, W. Hu, C. Chuang, S. Xie, A. Hu, W. Yan, X. Kong, X. Wu, H. Ji, L.-J. Wan, *J. Am. Chem. Soc.* **2019**, *141*, 3977.
- [82] Z.-Y. Wang, L. Wang, S. Liu, G.-R. Li, X.-P. Gao, *Adv. Funct. Mater.* **2019**, *29*, 1901051.
- [83] Z. Zhang, D. H. Wu, Z. Zhou, G. R. Li, S. Liu, X. P. Gao, *Sci. China Mater.* **2019**, *62*, 74.
- [84] Z.-Y. Wang, D.-D. Han, S. Liu, G.-R. Li, T.-Y. Yan, X.-P. Gao, *Electrochim. Acta* **2020**, *337*, 135772.
- [85] L. Wang, Z.-Y. Wang, J.-F. Wu, G.-R. Li, S. Liu, X.-P. Gao, *Nano Energy* **2020**, *77*, 105173.
- [86] S. Chen, Y. Ming, B. Tan, S. Chen, *Electrochim. Acta* **2020**, *329*, 135128.
- [87] Y. Pang, Y. Wen, W. Li, Y. Sun, T. Zhu, Y. Wang, Y. Xia, *J. Mater. Chem. A* **2017**, *5*, 17926.
- [88] S. Wang, J. Liao, X. Yang, J. Liang, Q. Sun, J. Liang, F. Zhao, A. Koo, F. Kong, Y. Yao, X. Gao, M. Wu, S.-Z. Yang, R. Li, X. Sun, *Nano Energy* **2019**, *57*, 230.
- [89] Q. Fan, W. Liu, Z. Weng, Y. M. Sun, H. L. Wang, *J. Am. Chem. Soc.* **2015**, *137*, 12946.
- [90] a) J. J. Cheng, L. F. Liu, S. W. Ou, Y. Ou, Q. Liu, H. J. Song, Y. Pan, *Mater. Chem. Phys.* **2019**, *224*, 384; b) K. Sun, D. Su, Q. Zhang, D. C. Bock, A. C. Marschilok, K. J. Takeuchi, E. S. Takeuchi, H. Gan, *J. Electrochem. Soc.* **2015**, *162*, A2834.
- [91] Z. Xiao, Z. Li, P. Li, X. Meng, R. Wang, *Nano Energy* **2020**, *70*, 104522.
- [92] a) A. Garsuch, S. Herzog, L. Montag, A. Krebs, K. Leitner, *ECS Electrochem. Lett.* **2012**, *1*, A24; b) L. Ma, S. Wei, H. L. Zhuang, K. E. Hendrickson, R. G. Hennig, L. A. Archer, *J. Mater. Chem. A* **2015**, *3*, 19857.
- [93] A. J. Jacobson, R. R. Chianelli, M. S. Whittingham, *J. Electrochem. Soc.* **1979**, *126*, 2277.
- [94] a) C. Niu, J. Meng, C. Han, K. Zhao, M. Yan, L. Mai, *Nano Lett.* **2014**, *14*, 2873; b) E. Baudrin, G. Sudant, D. Larcher, B. Dunn, J.-M. Tarascon, *Chem. Mater.* **2006**, *18*, 4369.
- [95] H. B. Wu, A. Pan, H. H. Hng, X. W. Lou, *Adv. Funct. Mater.* **2013**, *23*, 5669.
- [96] M. S. Whittingham, *Science* **1976**, *192*, 1126.
- [97] a) Y. Kim, S. Muhammad, H. Kim, Y.-H. Cho, H. Kim, J. M. Kim, W.-S. Yoon, *ChemSusChem* **2015**, *8*, 2378; b) K. E. Gregorczyk, A. C. Kozen, X. Chen, M. A. Schroeder, M. Noked, A. Cao, L. Hu, G. W. Rubloff, *ACS Nano* **2015**, *9*, 464.
- [98] a) C. Zhu, Y. Wen, P. A. van Aken, J. Maier, Y. Yu, *Adv. Funct. Mater.* **2015**, *25*, 2335; b) L. Fei, Q. Lin, B. Yuan, G. Chen, P. Xie, Y. Li, Y. Xu, S. Deng, S. Smirnov, H. Luo, *ACS Appl. Mater. Interfaces* **2013**, *5*, 5330.
- [99] a) D. Zhang, J. P. Tu, J. Y. Xiang, Y. Q. Qiao, X. H. Xia, X. L. Wang, C. D. Gu, *Electrochim. Acta* **2011**, *56*, 9980; b) T. B. Reddy, D. Linden, *Linden's Handbook of Batteries*, McGraw-Hill, New York **2011**.
- [100] a) X. Wang, Y. Wang, X. Li, B. Liu, J. Zhao, *J. Power Sources* **2015**, *287*, 185; b) Y. Wang, X. Zhang, P. Chen, H. Liao, S. Cheng, *Electrochim. Acta* **2012**, *80*, 264.
- [101] a) B. A. Trofimov, T. A. Skotheim, L. V. Andriyanova, A. G. Malkina, G. F. Myachina, S. A. Korzhova, T. I. Vakul'skaya, I. P. Kovalev, Y. V. Mikhailik, *Russ. Chem. Bull.* **1999**, *48*, 459; b) W. J. Chung, J. J. Griebel, E. T. Kim, H. Yoon, A. G. Simmonds, H. J. Ji, P. T. Dirlam, R. S. Glass, J. J. Wie, N. A. Nguyen, B. W. Guralnick, J. Park, Á. Somogyi, P. Theato, M. E. Mackay, Y.-E. Sung, K. Char, J. Pyun, *Nat. Chem.* **2013**, *5*, 518.
- [102] a) F. Wu, S. Chen, V. Srot, Y. Huang, S. K. Sinha, P. A. van Aken, J. Maier, Y. Yu, *Adv. Mater.* **2018**, *30*, 1706643; b) T. Takeuchi, T. Kojima, H. Kageyama, K. Mitsuhashi, M. Ogawa, K. Yamanaka, T. Ohta, H. Kobayashi, R. Nagai, A. Ohta, *J. Electrochem. Soc.* **2017**, *164*, A6288.
- [103] a) Y. Cui, A. Abouimrane, J. Lu, T. Bolin, Y. Ren, W. Weng, C. Sun, V. A. Maroni, S. M. Heald, K. Amine, *J. Am. Chem. Soc.* **2013**, *135*, 8047; b) A. Abouimrane, D. Dambournet, K. W. Chapman,

- P. J. Chupas, W. Weng, K. Amine, *J. Am. Chem. Soc.* **2012**, *134*, 4505; c) X. Li, J. Liang, K. Zhang, Z. Hou, W. Zhang, Y. Zhu, Y. Qian, *Energy Environ. Sci.* **2015**, *8*, 3181; d) J. Zhang, Z. Li, X. W. Lou, *Angew. Chem., Int. Ed.* **2017**, *56*, 14107.
- [104] a) K. Xu, X. Liu, J. Liang, J. Cai, K. Zhang, Y. Lu, X. Wu, M. Zhu, Y. Liu, Y. Zhu, G. Wang, Y. Qian, *ACS Energy Lett.* **2018**, *3*, 420; b) S. Li, Z. Han, W. Hu, L. Peng, J. Yang, L. Wang, Y. Zhang, B. Shan, J. Xie, *Nano Energy* **2019**, *60*, 153; c) J. Li, Y. Yuan, H. Jin, H. Lu, A. Liu, D. Yin, J. Wang, J. Lu, S. Wang, *Energy Storage Mater.* **2019**, *16*, 31; d) F. Sun, B. Zhang, H. Tang, Z. Yue, X. Li, C. Yin, L. Zhou, *J. Mater. Chem. A* **2018**, *6*, 10104.
- [105] C.-C. Chuang, Y.-Y. Hsieh, W.-C. Chang, H.-Y. Tuan, *Chem. Eng. J.* **2020**, *387*, 123904.
- [106] a) H. Ye, L. Ma, Y. Zhou, L. Wang, N. Han, F. Zhao, J. Deng, T. Wu, Y. Li, J. Lu, *Proc. Natl. Acad. Sci. USA* **2017**, *114*, 13091; b) X. Li, J. Liang, W. Li, J. Luo, X. Li, X. Yang, Y. Hu, Q. Xiao, W. Zhang, R. Li, T.-K. Sham, X. Sun, *Chem. Mater.* **2019**, *31*, 2002.
- [107] H. Yang, A. Naveed, Q. Li, C. Guo, J. Chen, J. Lei, J. Yang, Y. Nuli, J. Wang, *Energy Storage Mater.* **2018**, *15*, 299.
- [108] X. Wang, Y. Qian, L. Wang, H. Yang, H. Li, Y. Zhao, T. Liu, *Adv. Funct. Mater.* **2019**, *29*, 1902929.
- [109] Database of Computed Information on Known and Predicted Materials. <https://www.materialsproject.org/> (accessed: August 2020).
- [110] a) F. Sun, H. Cheng, J. Chen, N. Zheng, Y. Li, J. Shi, *ACS Nano* **2016**, *10*, 8289; b) J. Ding, H. Zhou, H. Zhang, L. Tong, D. Mitlin, *Adv. Energy Mater.* **2018**, *8*, 1701918.
- [111] a) G. S. Girolami, *J. Chem. Educ.* **1994**, *71*, 962; b) X. Cao, N. Leyva, S. R. Anderson, B. C. Hancock, *Int. J. Pharm.* **2008**, *355*, 231.
- [112] a) Z. Yuan, H.-J. Peng, J.-Q. Huang, X.-Y. Liu, D.-W. Wang, X.-B. Cheng, Q. Zhang, *Adv. Funct. Mater.* **2014**, *24*, 6105; b) F. Pei, L. Lin, D. Ou, Z. Zheng, S. Mo, X. Fang, N. Zheng, *Nat. Commun.* **2017**, *8*, 482; c) H. Shi, X. Zhao, Z.-S. Wu, Y. Dong, P. Lu, J. Chen, W. Ren, H.-M. Cheng, X. Bao, *Nano Energy* **2019**, *60*, 743; d) H. Pan, J. Chen, R. Cao, V. Murugesan, N. N. Rajput, K. S. Han, K. Persson, L. Estevez, M. H. Engelhard, J.-G. Zhang, K. T. Mueller, Y. Cui, Y. Shao, J. Liu, *Nat. Energy* **2017**, *2*, 813.
- [113] a) J.-L. Shi, H.-J. Peng, L. Zhu, W. Zhu, Q. Zhang, *Carbon* **2015**, *92*, 96; b) L. Qie, C. Zu, A. Manthiram, *Adv. Energy Mater.* **2016**, *6*, 1502459; c) G. Zhou, Y. Zhao, A. Manthiram, *Adv. Energy Mater.* **2015**, *5*, 1402263; d) Z. Zhang, Q. Li, K. Zhang, W. Chen, Y. Lai, J. Li, *J. Power Sources* **2015**, *290*, 159.
- [114] R. Fang, S. Zhao, P. Hou, M. Cheng, S. Wang, H.-M. Cheng, C. Liu, F. Li, *Adv. Mater.* **2016**, *28*, 3374.
- [115] a) S.-H. Chung, C.-H. Chang, A. Manthiram, *Energy Environ. Sci.* **2016**, *9*, 3188; b) G. Zhou, Y. Zhao, C. Zu, A. Manthiram, *Nano Energy* **2015**, *12*, 240; c) C.-H. Chang, S.-H. Chung, A. Manthiram, *Mater. Horiz.* **2017**, *4*, 249; d) S. H. Chung, A. Manthiram, *Joule* **2018**, *2*, 710; e) S.-H. Chung, C.-H. Chang, A. Manthiram, *ACS Nano* **2016**, *10*, 10462.
- [116] a) P. Xiao, F. Bu, G. Yang, Y. Zhang, Y. Xu, *Adv. Mater.* **2017**, *29*, 1703324; b) Y. Liu, G. Li, J. Fu, Z. Chen, X. Peng, *Angew. Chem., Int. Ed.* **2017**, *56*, 6176; c) C. Hu, C. Kirk, J. Silvestre-Albergo, F. Rodríguez-Reinoso, M. J. Biggs, *J. Mater. Chem. A* **2017**, *5*, 19924; d) Y. Mao, G. Li, Y. Guo, Z. Li, C. Liang, X. Peng, Z. Lin, *Nat. Commun.* **2017**, *8*, 14628.
- [117] M. Li, R. Carter, A. Douglas, L. Oakes, C. L. Pint, *ACS Nano* **2017**, *11*, 4877.
- [118] H. Pan, Z. Cheng, J. Chen, R. Wang, X. Li, *Energy Storage Mater.* **2020**, *27*, 435.
- [119] H. Xu, A. Manthiram, *Nano Energy* **2017**, *33*, 124.
- [120] H. Pan, K. S. Han, M. H. Engelhard, R. Cao, J. Chen, J.-G. Zhang, K. T. Mueller, Y. Shao, J. Liu, *Adv. Funct. Mater.* **2018**, *28*, 1707234.
- [121] a) Y. Yang, Y. Zhong, Q. Shi, Z. Wang, K. Sun, H. Wang, *Angew. Chem., Int. Ed.* **2018**, *130*, 15775; b) L. Peng, Z. Wei, C. Wan, J. Li, Z. Chen, D. Zhu, D. Baumann, H. Liu, C. S. Allen, X. Xu, A. I. Kirkland, I. Shakir, Z. Almutairi, S. Tolbert, B. Dunn, Y. Huang, P. Sautet, X. Duan, *Nat. Catal.* **2020**, *3*, 762.
- [122] Y. Q. Tao, Y. J. Wei, Y. Liu, J. T. Wang, W. M. Qiao, L. C. Ling, D. H. Long, *Energy Environ. Sci.* **2016**, *9*, 3230.
- [123] a) G. M. Zhou, H. Z. Tian, Y. Jin, X. Y. Tao, B. F. Liu, R. F. Zhang, Z. W. Seh, D. Zhuo, Y. Y. Liu, J. Sun, J. Zhao, C. X. Zu, D. S. Wu, Q. F. Zhang, Y. Cui, *Proc. Natl. Acad. Sci. USA* **2017**, *114*, 840; b) J. Pu, Z. Shen, J. Zheng, W. Wu, C. Zhu, Q. Zhou, H. Zhang, F. Pan, *Nano Energy* **2017**, *37*, 7.
- [124] a) Y. R. Zhong, L. C. Yin, P. He, W. Liu, Z. S. Wu, H. L. Wang, *J. Am. Chem. Soc.* **2018**, *140*, 1455; b) J. H. Cheng, D. Zhao, L. S. Fan, X. Wu, M. X. Wang, N. Q. Zhang, K. N. Sun, *J. Mater. Chem. A* **2017**, *5*, 14519; c) S. Huang, Y. V. Lim, X. Zhang, Y. Wang, Y. Zheng, D. Kong, M. Ding, S. A. Yang, H. Y. Yang, *Nano Energy* **2018**, *51*, 340.
- [125] a) L. Ma, H. Yuan, W. Zhang, G. Zhu, Y. Wang, Y. Hu, P. Zhao, R. Chen, T. Chen, J. Liu, Z. Hu, Z. Jin, *Nano Lett.* **2017**, *17*, 7839; b) T.-G. Jeong, D. S. Choi, H. Song, J. Choi, S.-A. Park, S. H. Oh, H. Kim, Y. Jung, Y.-T. Kim, *ACS Energy Lett.* **2017**, *2*, 327.
- [126] a) Y. Zhang, Z. Mu, C. Yang, Z. Xu, S. Zhang, X. Zhang, Y. Li, J. Lai, Z. Sun, Y. Yang, Y. Chao, C. Li, X. Ge, W. Yang, S. Guo, *Adv. Funct. Mater.* **2018**, *28*, 1707578; b) F. Zhou, Z. Li, X. Luo, T. Wu, B. Jiang, L.-L. Lu, H.-B. Yao, M. Antonietti, S.-H. Yu, *Nano Lett.* **2018**, *18*, 1035.
- [127] J. Liang, L. C. Yin, X. N. Tang, H. C. Yang, W. S. Yan, L. Song, H. M. Cheng, F. Li, *ACS Appl. Mater. Interfaces* **2016**, *8*, 25193.
- [128] J.-J. Chen, R.-M. Yuan, J.-M. Feng, Q. Zhang, J.-X. Huang, G. Fu, M.-S. Zheng, B. Ren, Q.-F. Dong, *Chem. Mater.* **2015**, *27*, 2048.
- [129] Z.-L. Xu, S. Lin, N. Onofrio, L. Zhou, F. Shi, W. Lu, K. Kang, Q. Zhang, S. P. Lau, *Nat. Commun.* **2018**, *9*, 4164.
- [130] Q. Pang, X. Liang, C. Y. Kwok, L. F. Nazar, *Nat. Energy* **2016**, *1*, 16132.
- [131] a) E. Gülzow, M. Schulze, N. Wagner, T. Kaz, R. Reissner, G. Steinhilber, A. Schneider, *J. Power Sources* **2000**, *86*, 352; b) E. Gülzow, T. Kaz, *J. Power Sources* **2002**, *106*, 122.
- [132] H. Duong, J. Shin, Y. Yudi, presented at 48th Power Sources Conference, Denver, CO June **2018**.
- [133] a) D.-W. Park, N. A. Cañas, N. Wagner, K. A. Friedrich, *J. Power Sources* **2016**, *306*, 758; b) B. Ludwig, Z. Zheng, W. Shou, Y. Wang, H. Pan, *Sci. Rep.* **2016**, *6*, 23150.
- [134] S. Thieme, J. Brückner, I. Bauer, M. Oschatz, L. Borchardt, H. Althues, S. Kaskel, *J. Mater. Chem. A* **2013**, *1*, 9225.
- [135] F. Hippauf, B. Schumm, S. Doerfler, H. Althues, S. Fujiki, T. Shiratsuchi, T. Tsujimura, Y. Aihara, S. Kaskel, *Energy Storage Mater.* **2019**, *21*, 390.
- [136] L. Cheng, L. A. Curtiss, K. R. Zavadil, A. A. Gewirth, Y. Shao, K. G. Gallagher, *ACS Energy Lett.* **2016**, *1*, 503.
- [137] a) H. Pan, K. S. Han, M. Vijayakumar, J. Xiao, R. Cao, J. Chen, J. Zhang, K. T. Mueller, Y. Shao, J. Liu, *ACS Appl. Mater. Interfaces* **2017**, *9*, 4290; b) H. Chu, H. Noh, Y.-J. Kim, S. Yuk, J.-H. Lee, J. Lee, H. Kwack, Y. Kim, D.-K. Yang, H.-T. Kim, *Nat. Commun.* **2019**, *10*, 188; c) H. Chu, J. Jung, H. Noh, S. Yuk, J. Lee, J.-H. Lee, J. Baek, Y. Roh, H. Kwon, D. Choi, K. Sohn, Y. Kim, H.-T. Kim, *Adv. Energy Mater.* **2020**, *10*, 2000493.



Ya-Tao Liu is going to pursue a postdoctoral research in College of Engineering, Peking University. He received his Ph.D. in 2019 from the School of Materials Science and Engineering, Nankai University. He has focused his research on developing new materials for energy storage technology, with a special interest in lithium–sulfur batteries.



Xue-Ping Gao is a professor in Institute of New Energy Material Chemistry, Nankai University of China. He received his doctorate at Department of Chemistry from Nankai University in 1995. He used to work as a visiting research fellow at Kogakuin University in Japan from 1997 to 1999. Currently, his main research is focused on energy storage materials for power sources, including Li–S batteries, Li-ion batteries, and solar rechargeable batteries.